

# SPICE Modeling of Magnetic Components

## Introduction

Magnetic components are a vital part of most power electronic equipment, and the models used in a simulation must faithfully reproduce or predict the behavior of the circuit. Most of the other electronic components in these circuits have predetermined models that have been derived from standardized components. Magnetic components, however, are rarely standardized and are generally designed for specific applications. In most cases the model, or at least the component values within the model, must be altered for each new circuit simulation.

PSpice has four basic magnetic component models built into it:

- A linear inductor
- An ideal transformer
- A coupled inductor model
- A nonlinear core model

All of these are very useful for simulation but must be used with some care if the correct model is to be obtained.

In some cases, the model may fail dramatically, thereby giving grossly erroneous results, as we shall see later. Most of the time, however, the errors are more subtle. For example, the details of the noise and ringing due to parasitics in the transformer may not be reproduced correctly. Cross-regulation between windings with varying loads, high-frequency winding losses, and the proper distribution of ripple currents in coupled filter inductors are also quantities that are often not modeled accurately.

## Basic Transformer Types

### Junction Transformer

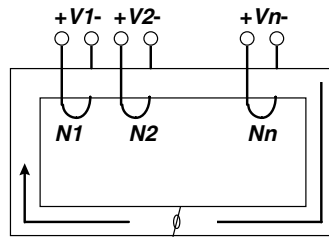
$$\frac{v_1}{n_1} = \frac{v_2}{n_2} = \dots = \frac{v_n}{n_n}$$

$$n_1 i_1 + n_2 i_2 + \dots + n_n i_n = 0$$

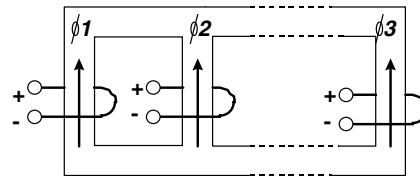
### Mesh Transformer

$$\frac{v_1}{n_1} + \frac{v_2}{n_2} + \dots + \frac{v_n}{n_n} = 0$$

$$n_1 i_1 = n_2 i_2 = \dots = n_n i_n$$



Junction Transformer



Mesh Transformer

**Figure 2.1** Two basic transformer types.

These problems usually arise from shortcomings in the models that are being used and can, for the most part, be corrected.

A common modeling problem arises because of a failure to realize that there are *two* different basic types of transformers: junction and mesh. Figure 2.1 illustrates these two transformer types, along with the circuit equations that apply to each type.

The junction transformer is widely used in power conversion equipment. It is usually the type used by schematic capture programs and is also used to create ideal transformers having multiple windings.

The mesh transformer is very common for polyphase power applications and also appears in coupled filter inductors and other magnetic control devices. There are also magnetic devices that are combinations of mesh and junction transformers. In a network, these two types of transformers behave very differently. The substitution of one for the other in a simulation will lead to gross errors, as shown in the example in Fig. 2.2.

This is a three-winding, three-leg mesh transformer. If a simple three-winding ideal transformer (Fig. 2.2, upper right) is selected to simulate this transformer, the output voltage phases will be correct only for some excitations. If, for example, the center winding is excited, then the voltages on the other two windings will be correct. However, if one of the

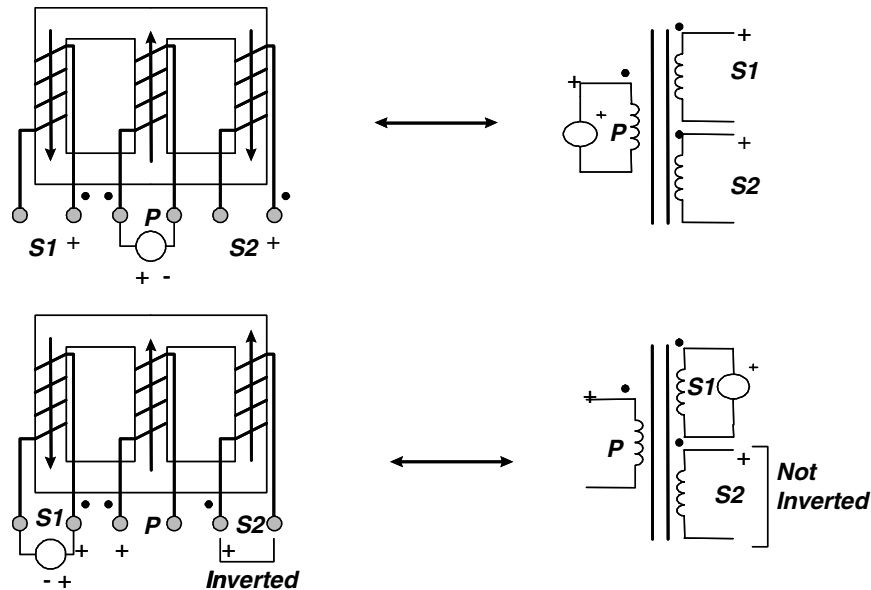


**Figure 2.2** Modeling of mesh transformers requires caution. The example above shows how errors can be easily made.

outer leg windings is excited, as shown in the bottom left of Fig. 2.2, then the phase of the simulated voltage (bottom right of Fig. 2.2) will be incorrect. This represents a gross modeling error and illustrates why the modeling must be performed carefully. The selected model will function correctly as a junction transformer, but it will not function correctly as a mesh transformer.

Most simulation problems can be avoided by using models that are extensions of the basic SPICE models. The most reliable way to create these models is to base them on the actual physical structure of the magnetic component. This is the principle behind the physical models that are derived using reluctance modeling and are described in the Reluctance and Physical Models section. This approach has many advantages beyond the simple generation of a model. Physical models preserve the relationship between the simulation model and the actual component. This means, for example, if the simulation shows excessive voltage ringing due to a parasitic inductance element, this component can be directly related to the structure of the device. This allows the device to be redesigned in order to reduce the problem. This interchange between the simulation and the device design is a powerful tool. The preservation of the intuitive connections between the device and the simulation model also helps to avoid modeling errors and to interpret the simulation results.

## Ideal Components in SPICE

### Passive components

The built-in models in SPICE provide reasonable first-order approximations for circuit behavior. Unfortunately, most circuits must be designed to be tolerant of second-order effects, at a minimum, and must occasionally provide compensation in order to achieve a desired performance level. Most frequently, the parasitic and second-order effects are related to changes in frequency.

It may not be clear, especially to novice SPICE users, that when you use a passive component, such as an inductor or a capacitor, you are using an *ideal* element. Parasitics, such as equivalent series resistance (ESR) or parasitic inductance, are not included. This is done intentionally in order to allow you to take advantage of the ideal nature of these elements. However, parasitics can both dominate and plague a circuit design. Therefore, accurate representations are an essential part of a realistic simulation.

Electronic circuits are always modeled over a finite range of the electromagnetic frequency spectrum. There is no need to describe operation of electrical components from DC through the RF, microwave, optical, X-ray, and gamma-ray spectrums. Not only would the model be complex, but it would be inaccurate and would provide unnecessary information.

The nodal equations that SPICE solves are valid only when the circuit elements are small as compared with the wavelength of the highest frequency of interest (high frequencies are limited below the optical band). Even with this limitation, the useful frequency range runs from millihertz to many gigahertz, over 15 orders of magnitude. The reactance chart of Fig. 2.3 shows the expected range of parasitic inductance and capacitance over this range. The darkly shaded region represents the values of impedances that are realistically achieved with common R-L-C components and printed circuit board technology. The lightly shaded region of impedances can be viewed as a transition region where parasitics become increasingly important. The boundary between the lightly shaded region and the unshaded region represents the smallest capacitance or inductance parasitic value, and therefore values in the unshaded area are unrealistic for single discrete components. At the high-frequency end, this suggests the use of smaller geometry microwave integrated circuits, while the extension of the impedance range at lower frequencies requires larger geometries than are ordinarily found in PC card technology.

The modeling additions for various components are shown in the pictorial inlays. First, resistors, which are basically defined at DC, turn into effective capacitors or inductors; their impedance converges to that of free space divided by the square root of the dielectric constant,

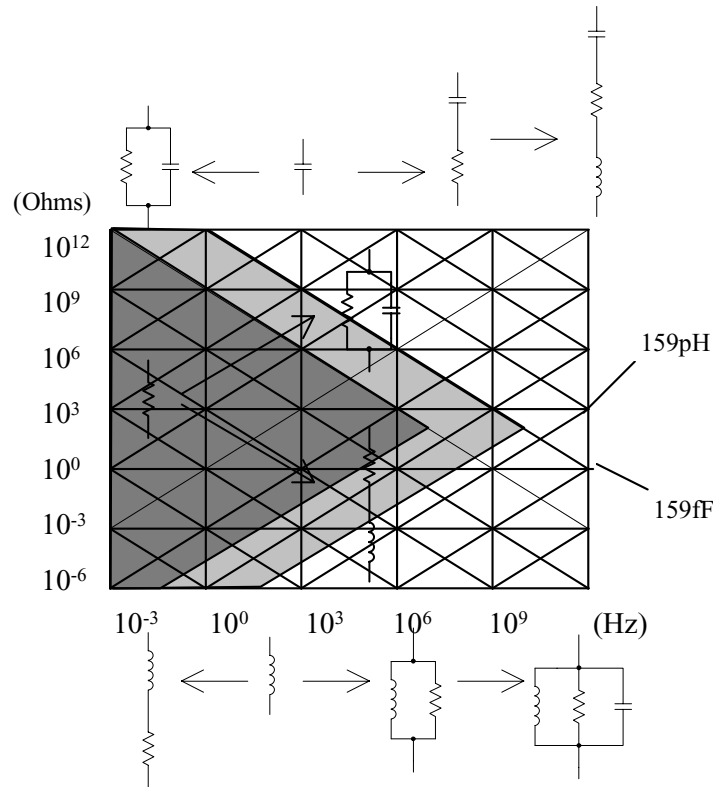


Figure 2.3 Reactance chart for modeling R-L-C components.

something in the neighborhood of  $125 \Omega$  for PC cards. Similarly, capacitor and inductor impedances funnel toward the impedance of the propagating medium at high frequencies and become resistive as the frequency approaches DC.

### Transformers

The usual method of simulating a transformer using SPICE is via the specification of the open-circuit inductance that is seen at each winding, and then the addition of the coupling coefficients to a pair of coupled inductors. This technique tends to lose the physical meaning associated with leakage and magnetizing inductance and does not allow the insertion of a nonlinear core. It does, however, provide a transformer that is simple to create and simulates efficiently. The coupled inductor type of transformer, its related equations, and its relationship to an ideal transformer with added leakage and magnetizing inductance are discussed in the next section.

22 Chapter Two

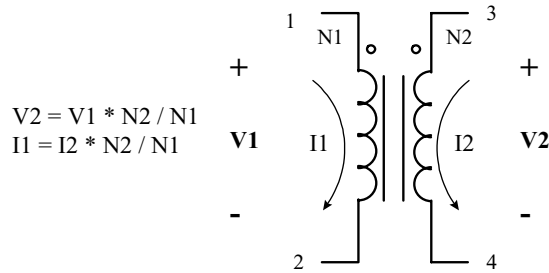


Figure 2.4 Ideal transformer with its voltage and current relationships.

To make a transformer model that more closely represents the physical processes, it is necessary to construct an ideal transformer and model the magnetizing and leakage inductances separately. The ideal transformer is one that preserves the voltage and current relationships shown in Fig. 2.4 and has a unity coupling coefficient and infinite magnetizing inductance. The ideal transformer, unlike a real transformer, will operate at DC. This is a property that is useful for modeling the operation of DC-to-DC converters.

The SPICE subcircuit for the ideal transformer is sometimes called XFMR. The TURNS subcircuit performs a similar function with the exception that the Ratio parameter is equal to 1/NUM (the number of turns).

The SPICE equivalent circuit is shown in Fig. 2.5, and it implements the following equations:

$$V_1 * \text{ratio} = V_2$$

$$I_1 = I_2 * \text{ratio}$$

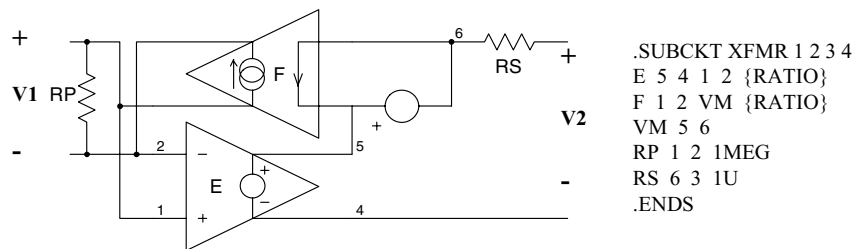


Figure 2.5 The ideal transformer (XFMR or TURNS) model allows operation at DC and the addition of magnetizing and leakage inductances, as well as a saturable core, in order to make a complete transformer model. Parameter passing allows the transformer to simulate any turns ratio.

RP and RS are used to prevent singularities in applications where terminals 1 and 2 are open circuit or terminals 3 and 4 are connected to a voltage source. RATIO is the turns ratio from winding 1, 2 to winding 3, 4. The polarity “dots” are on terminals 1 and 3. Multiwinding topologies can be simulated using combinations of this two-port representation [3,4].

### PSpice Coupled Inductor Model

The coupled inductor model is a classical network representation for a transformer. As shown in Fig. 2.6, the model assumes that a transformer can be represented by an inductor for each winding ( $L_1, L_2, \dots, L_n$ ) and a series of mutual inductances between the windings ( $M_{12}, M_{13}, \dots, M_{1n}, \dots, M_{nn}$ ).

*Note:* In PSpice, if all the inductor couplings have the same value the coupling element may also be written as Kall L1 L2 L3 *Couple\_value*.

In matrix form, this is expressed as

$$\begin{bmatrix} V_1 \\ \cdot \\ \cdot \\ \cdot \\ V_n \end{bmatrix} = \begin{bmatrix} L_{11} & \cdot & M_{1j} & \cdot & M_{1n} \\ \cdot & L_{22} & \cdot & \cdot & \cdot \\ \cdot & \cdot & \cdot & \cdot & \cdot \\ \cdot & \cdot & \cdot & \cdot & \cdot \\ M_{n1} & \cdot & \cdot & \cdot & L_{nn} \end{bmatrix} \begin{bmatrix} \left(\frac{di_1}{dt}\right) \\ \cdot \\ \cdot \\ \cdot \\ \left(\frac{di_n}{dt}\right) \end{bmatrix} \quad (2.1)$$

Algebraically, the two-winding transformer equations would be

$$\begin{aligned} v_1 &= (L_1) \frac{di_1}{dt} + (M_{12}) \frac{di_2}{dt} \\ v_2 &= (M_{12}) \frac{di_1}{dt} + (L_2) \frac{di_2}{dt} \end{aligned} \quad (2.2)$$

```
L1 4 5 1uH
L2 6 7 2uH
L3 8 9 3uH
K12 L1 L2 .999
K23 L2 L3 .950
K13 L1 L3 .995
```

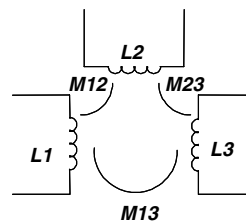


Figure 2.6 SPICE coupled inductor model and associated netlist.

24 Chapter Two

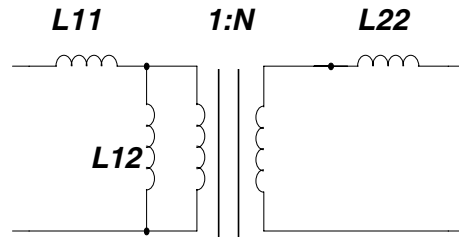


Figure 2.7 Structure of the Pi model.

Mutual inductance can be expressed in alternative form using coefficients of coupling,  $k_{ij}$ . A typical example would be

$$k_{12} = \frac{M_{12}}{\sqrt{L_1 L_2}} \quad (2.3)$$

In a transformer,  $k_{ij}$  will normally be very close to 1. A typical PSpice listing for a coupled inductor is shown in Fig. 2.6.

This is an abstract model. Most engineers, however, will be thinking in terms of a circuit model that has leakage and magnetizing inductance and a turns ratio. An example of this type of model is shown in Fig. 2.7.

The circuit equations for this model are

$$\begin{aligned} v_1 &= (L_{11} + L_{12}) \frac{di_1}{dt} + (n L_{12}) \frac{di_2}{dt} \\ v_2 &= (n L_{12}) \frac{di_1}{dt} + (L_{22} + n^2 L_{12}) \frac{di_2}{dt} \end{aligned} \quad (2.4)$$

The relationship between the two models is

$$\begin{aligned} L_1 &= L_{11} + L_{12} \\ L_2 &= L_{22} + n^2 L_{12} \\ M_{12} &= n L_{12} \\ k_{12} &= \frac{n L_{12}}{\sqrt{(L_{11} + L_{12})(L_{22} + n^2 L_{12})}} \end{aligned} \quad (2.5)$$

To use the coupled inductor model, it is necessary to first determine the values in the Pi model and then convert them to the values for the coupled inductor model. For two- or three-winding transformers, this is a straightforward process, but when four or more windings are used, the conversion relationships become quite complex. In these cases, it is



better to stay with the physical model and implement it using the ideal components that are available in PSpice.

There may be another problem with the coupled inductor model. In a typical transformer, the magnetizing inductance ( $L_{12}$ ) might be 5 mH. The leakage inductances may be only  $0.5 \mu\text{H}$ . The value of  $k$  must be specified with enough accuracy to recreate this difference accurately; that is, a difference of  $10^4$ . For  $n = 1$ ,  $k_{12} = 0.99990$  for the preceding values. Inversion of Eq. (2.5) illustrates the problem:

$$\begin{aligned} L_{11} &= L_1 - \frac{k_{12}}{n} \sqrt{L_1 L_2} \\ L_{22} &= L_2 - nk_{12} \sqrt{L_1 L_2} \\ L_{12} &= \frac{k_{12}}{n} \sqrt{L_1 L_2} \end{aligned} \quad (2.6)$$

$L_{11}$  and  $L_{22}$  are the small difference between two large numbers. In general, you should compute  $k_{i,j}$  to four decimal places.

### Reluctance and Physical Models

The basic problem when simulating a magnetic component is to translate the physical structure of the device into an equivalent electric circuit. PSpice will use the equivalent circuit to simulate the device. Reluctance modeling, combined with a duality transformation, provides a means to accomplish this task. Reluctance modeling creates a magnetic circuit model that can then be converted into an electric circuit model.

Table 2.1 shows a number of analogous quantities between electric and magnetic circuits.

By comparing the form of the equations in each column, the following analogous quantities can be identified:

- EMF ( $V$ ) and MMF ( $F$ )
- Electric field ( $E$ ) and magnetic field ( $H$ ) intensities
- Current density ( $J$ ) and flux density ( $B$ )
- Current ( $I$ ) and flux ( $\phi$ )
- Resistance ( $R$ ) and reluctance ( $R'$ )
- Conductivity ( $\sigma$ ) and permeability ( $\mu$ )

Reluctance is computed in the same manner as resistance, that is, from the dimensions of the magnetic path and the magnetic conductivity ( $\mu$ ).

26 Chapter Two

**TABLE 2.1 Electric and Magnetic Circuit Analogous Quantities**

Electric	Magnetic
$V \equiv$ electric circuit voltage (Electromotive force)	$F \equiv NI =$ magnetic circuit voltage (magnetomotive force)
$E \equiv$ electric field intensity	$H \equiv$ magnetic field intensity
$V = -\int \vec{E} \cdot d\vec{l}_c = El_c$	$F = \oint \vec{H} \cdot d\vec{l}_m = Hl_m$
$E = \frac{V}{l_c}$	$H = \frac{F}{l_m} = \frac{NI}{l_m}$
$J \equiv$ current density	$B \equiv$ magnetic flux density
$J = \sigma E$	$B = \mu H$
$\sigma =$ conductivity	$\mu =$ permeability $\mu_0 = 4\pi \times 10^{-7}$ H/m
$I \equiv$ electric current	$\phi \equiv$ magnetic flux
$I = -\int_s \vec{J} \cdot d\vec{s} = JA_c$	$\phi = \int_s \vec{B} \cdot d\vec{s} = BA_m$
$R =$ resistance	$R' =$ reluctance
$R = \frac{V}{I} = \frac{l_c}{\sigma A_c}$	$R' = \frac{F}{\phi} = \frac{l_m}{\mu A_m} = \frac{N^2}{L}$
$G = 1/R =$ conductance	$P = 1/R' =$ permeance

For a constant cross-sectional area ( $A_m$ ), the reluctance is

$$R' = \frac{l_m}{\mu A_m} \quad (2.7)$$

where  $\mu = \mu_0 \mu_r$

$\mu_r =$  relative permeability

The inductance of a magnetic circuit is directly related to  $R$  and  $N$  (the number of winding turns):

$$L = \frac{N^2}{R} = N^2 P \quad (2.8)$$

and

$$M_{12} = \frac{N_1 N_2}{N_{12}} = N_1 N_2 P_{12}$$

where  $P =$  permeance  $= 1/R'$ .

The example in Fig. 2.8 illustrates the development of the reluctance model for a simple inductor with an air gap in the core. The model develops as follows:

- Divide the core, including the air gaps, into sections and assign a reluctance to each one (as shown in Fig. 2.8B).
- Compute the reluctance for each section.
- Assign a magnetic voltage source to the winding with  $F = NI$ .
- Draw the equivalent network as shown in Fig. 2.9.

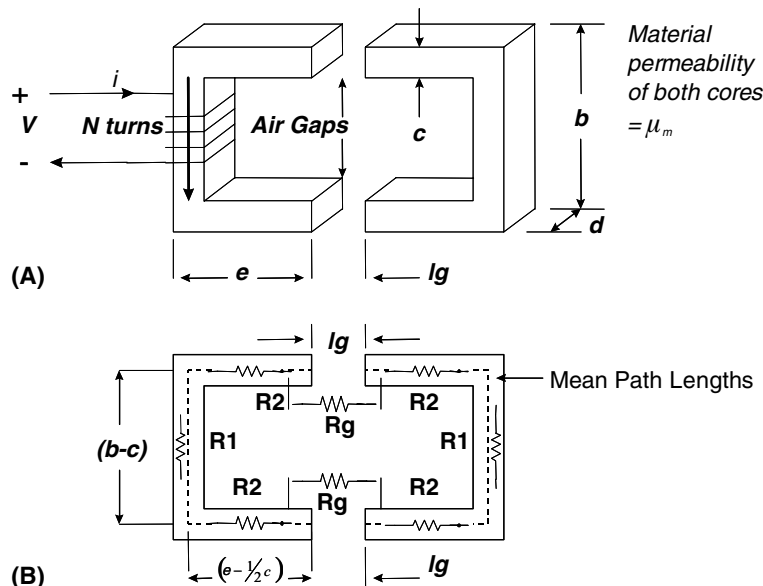


Figure 2.8 The development of the reluctance model for a simple inductor with an air gap.

Figure 2.9 is the reluctance model that represents the magnetic structure at the top of Fig. 2.8.

Now we need to convert this reluctance model to an equivalent electric circuit model, but before we can do that, it will help to briefly review the duality transformation. We can then proceed to convert the reluctance model.

An example of a duality transformation is given in Fig. 2.10. A node is placed within each mesh, including the outer mesh. Branches, which

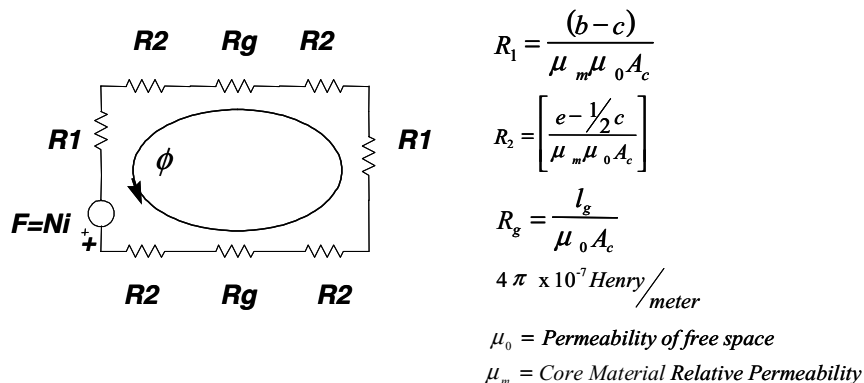


Figure 2.9 Reluctance model for the inductor in Fig. 2.8.

28 Chapter Two

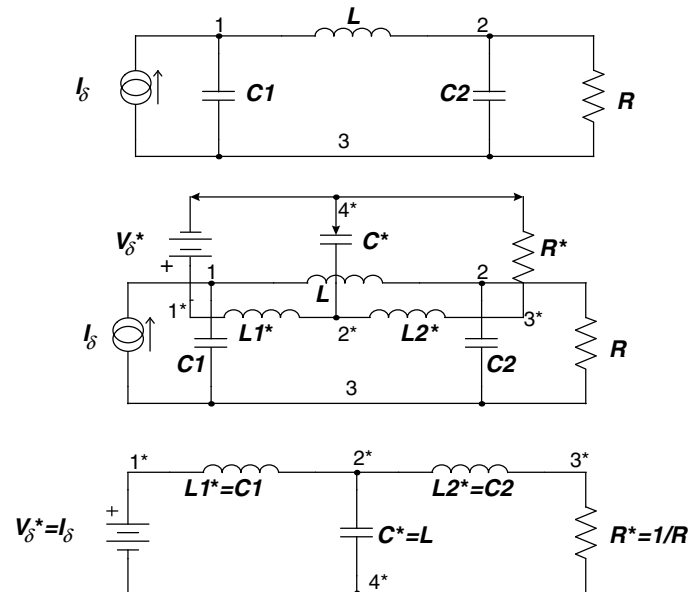


Figure 2.10 Review of the duality transform process.

intersect each of the branches in the original network, are connected between each node. In each of the intersecting branches, current and voltage are interchanged. The result is a new network that is the topological and electrical dual of the original network. A listing of dual quantities is given in Table 2.2.

TABLE 2.2 Duality Relationships

Quantity	Dual element
$V$	$I^*$
$I$	$V^*$
$q$	$\phi^*$
$\phi$	$q^*$
$R$	$R^* = G = 1/R$
$G$	$G^* = R = 1/G$
$C$	$L^*$
$L$	$C^*$
Open circuit	Short circuit
Short circuit	Open circuit
$D$	$D^* = 1 - D$
Voltage generator	Current generator
Current generator	Voltage generator
Mesh	Node
Node	Mesh

The conversion from a reluctance model to a circuit model requires the following steps:

- Draw the reluctance ( $R'$ ) model from the device structure and an estimate of the flux paths.
- Using duality, convert the  $R'$  model to a permeance ( $P$ ) model.
- Scale the  $P$  model for the winding turns by multiplying  $P$  by  $N$ .
- Scale this model for the winding voltage by multiplying again by  $N$ .
- Replace the scaled permeances with inductors.
- For multiple windings, use ideal transformers in order to provide the correct voltages.

A simple example shows how this process works. Keep in mind that the objective is to convert the physical model, which is in terms of magnetic quantities associated with the actual structure, to an electrical model, which is in terms of lumped inductances, ideal transformers, and winding voltages and currents. This is the model we want to use in the simulation. In Fig. 2.11A, the reluctance network has been simplified by combining the material reluctances into one element and the air gap reluctances into another. Figure 2.11B is the dual network in which reluctances have become permeances, the magnetic current ( $\phi$ )

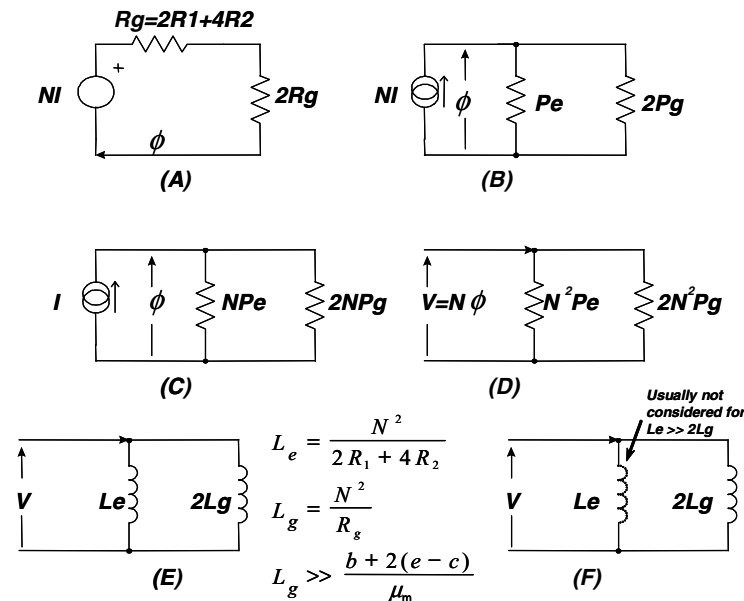


Figure 2.11 Reluctance modeling example.

30 Chapter Two

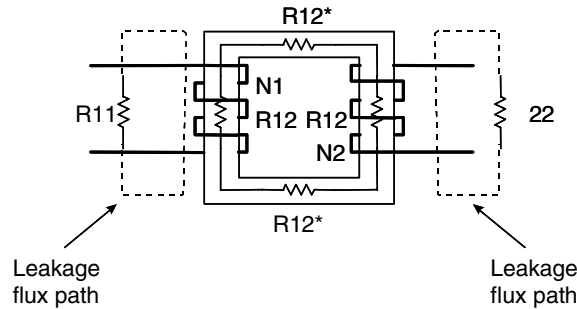


Figure 2.12 A two-winding transformer.

has become a magnetic voltage, the magnetic voltage source has become a magnetic current source, and series branches have become parallel branches.

The next step, Fig. 2.11C, is to scale the network in order to remove  $N$  from the current source, thereby leaving only the winding current,  $I$ .  $\phi$  must be kept constant; the multiplication of the current source by  $1/N$  implies that each of the permeances must be multiplied by  $N$ .

The winding voltages are introduced by invoking Faraday's law,  $V = N\phi$ . Each element in the network is now multiplied by  $N$ , as shown in Fig. 2.11D. The resulting network is now in terms of the winding voltage and the permeances scaled by  $N^2$ . From Eq. (2.8), we know that  $L = N^2P$ , so that the scaled permeances can be replaced by inductances (as shown in Fig. 2.11E and F).

We can now apply this process to a two-winding transformer like that shown in Fig. 2.12. The reluctance model, which is shown in Fig. 2.13, includes a voltage source for each winding ( $N_1$  and  $N_2$ ), a reluctance for the common flux path ( $R_{12}$ ), and reluctances for the

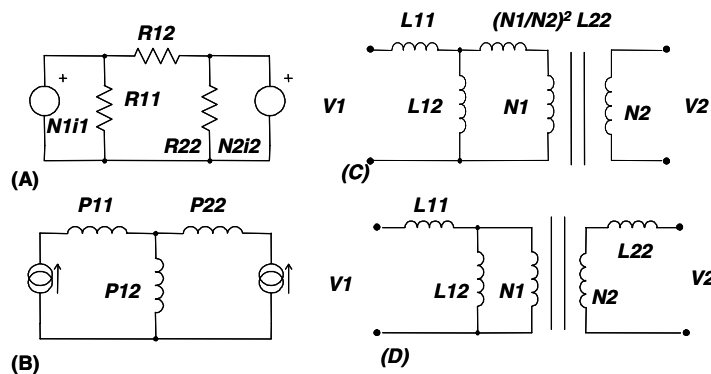


Figure 2.13 Reluctance model for a two-winding transformer.

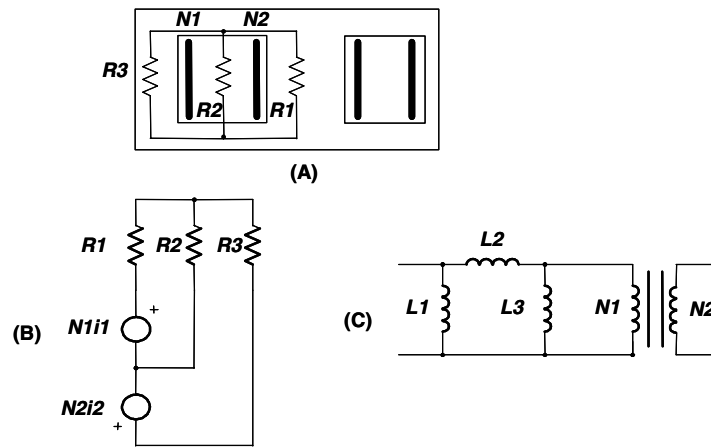


Figure 2.14 A realistic transformer model with multiple layers on the center leg of an E-E core.

leakage flux associated with each winding ( $R_{11}$  and  $R_{22}$ ). The reluctance model is transformed into a permeance model in Fig. 2.13B. This model is then scaled using  $N_1$  as the reference winding, and inductances are inserted as shown in Fig. 2.13C. The transformer turns ratio is maintained via the use of an ideal transformer. This is the well-known Pi model. As shown in Fig. 2.13D,  $L_{22}$  can be moved to the secondary by scaling by the square of the turns ratio ( $N_2^2/N_1^2$ ).

The transformer shown in Fig. 2.12 is easy to understand but reflects a physical structure that is rarely used. A much more common transformer structure takes the form of multiple layers on a common bobbin, on the center leg of an E-E core.

A cross section of such a transformer is shown in Fig. 2.14A, along with reluctances that represent the core ( $R_1$  and  $R_3$ ) and the leakage flux between the windings ( $R_2$ ). The corresponding reluctance model and the final circuit model are shown in Fig. 2.14B and C. Note that this model is different from the previous one (Fig. 2.13C). In the case of two windings, the two models can be shown to be equivalent using a delta-wye transform. When four or more windings are present, however, the model does not typically reduce to the Pi model. In fact, the Pi model is not valid for transformers with more than three windings.

The extension of Fig. 2.14 to an  $n$ -layer transformer is shown in Fig. 2.15. In the typical case, where the magnetizing inductances are large compared with the leakage inductances, the numerous shunt

32 Chapter Two

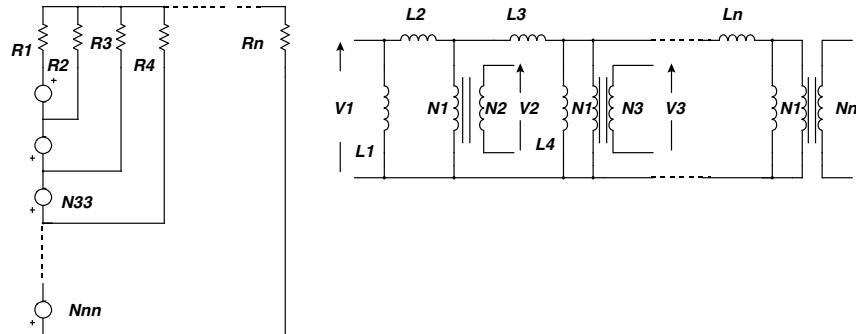


Figure 2.15 Extension of the reluctance generated circuit model to an  $n$ -layer transformer.

magnetizing inductors can be replaced with a single shunt inductance, as shown in Fig. 2.16.

- In most cases, the multiple magnetizing inductors in an  $n$ -winding transformer can be reduced to a single equivalent without any great error.
- An exception would be the case where there is an air gap on an outer leg or a magnetic shunt is present.

Note that this model performs equally well for transformers with interleaved winding layers. The layers that represent each winding are simply connected in series in order to make the final model.

Even though this model is more complex than the simple Pi model, it has the major advantage of correctly placing the leakage impedances with respect to the windings. This helps to make the simulation of cross-regulation, under varying winding loads, much more accurate in a multiple-winding transformer.

Using this modeling process, more and more details from the physical structure can be added to the model. The problem, however, is that the model may become very complex. This makes it more difficult to use. In general, the simplest possible model that gives acceptable results

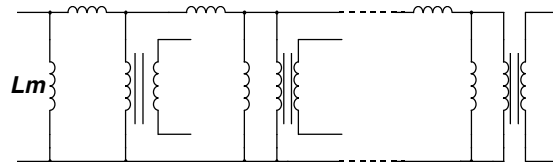
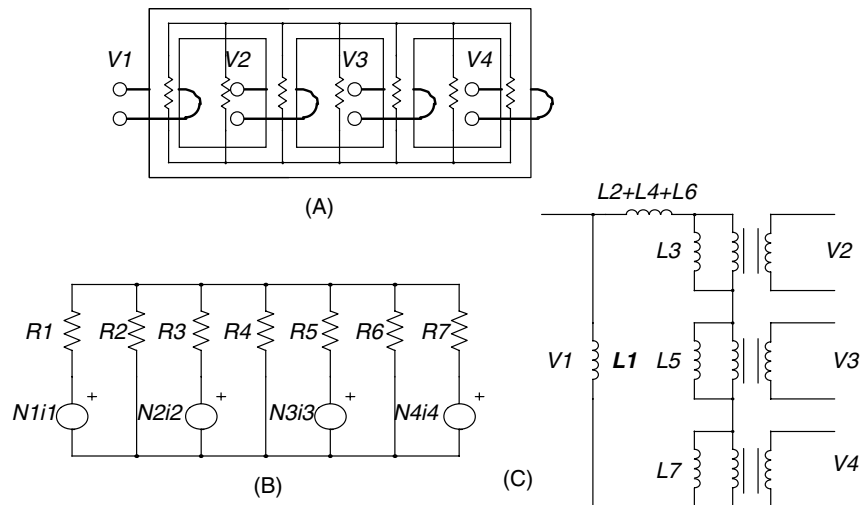


Figure 2.16 Eliminating multiple magnetizing inductance elements.





**Figure 2.17** A four-winding mesh transformer (A), along with its reluctance model (B), and the resulting equivalent circuit (C).

should be used, and complex models should be avoided whenever possible. The need for a complex model depends entirely upon how accurately the small details of the device performance need to be modeled and how willing you are to develop the necessary model.

The following examples show more complex applications of reluctance modeling.

Figure 2.17 gives an example of a four-winding mesh transformer that might be used in a polyphase power system. The reluctance modeling proceeds as shown previously and results in the model given in Fig. 2.17C. Note how different this model is from an equivalent four-winding junction transformer. Instead of cascaded parallel windings, the windings are in series. This is because mesh and junction transformers are topological duals.

Integrated magnetic structures that incorporate transformers and inductors into a common structure are becoming more common. An example of an integrated magnetic forward converter is given in Fig. 2.18a. A sketch of the magnetic structure is given in Fig. 2.18b. The reluctance model and the series of steps required to convert it to a circuit model are shown in Fig. 2.19. Again, the process is exactly as shown earlier; however, it is more complex now. The completed model, which has been inserted back into the circuit simulation, is shown in Fig. 2.20.

Using the reluctance modeling procedure, the derivation of an appropriate model is straightforward, although a bit tedious. Without this process, the appropriate model is far from obvious.

34 Chapter Two

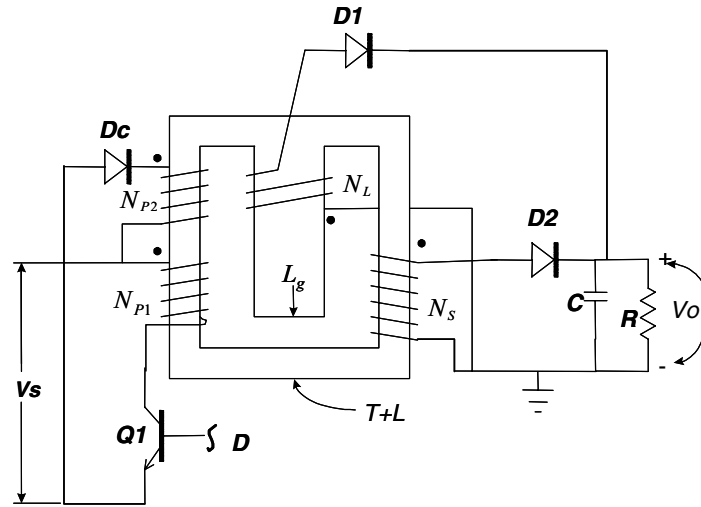


Figure 2.18a. An integrated magnetic forward converter circuit.

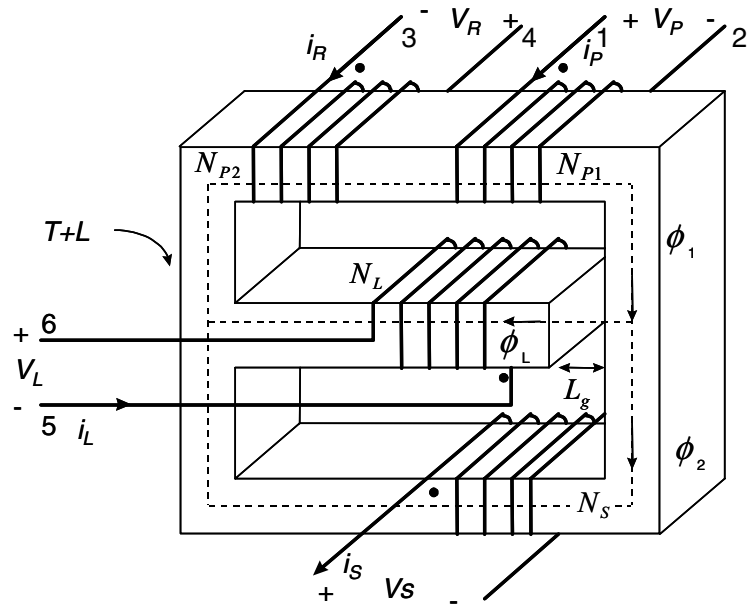
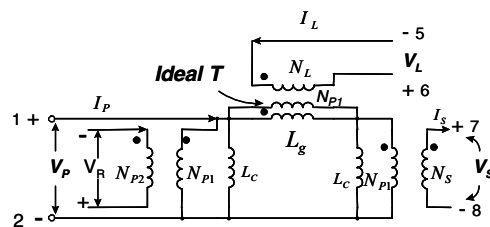
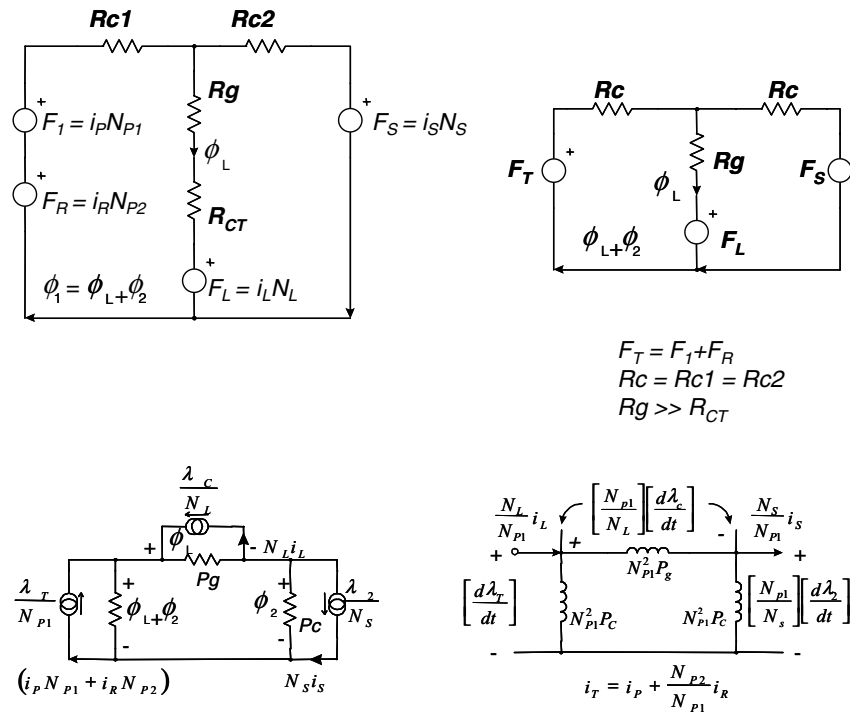


Figure 2.18b. The magnetic structure used in the integrated forward converter.



**Figure 2.19** The reluctance modeling procedure for the transformer used in the forward converter.

### Saturable Core Modeling

It would be difficult to accurately model power circuits without the ability to model magnetics. This section details the SPICE 2 and SPICE 3 methods that are used to simulate various types of magnetic cores including molypermalloy powder (MPP) and ferrite. The presented techniques can be extended to many other types of cores, such as tape wound, amorphous metal, etc.

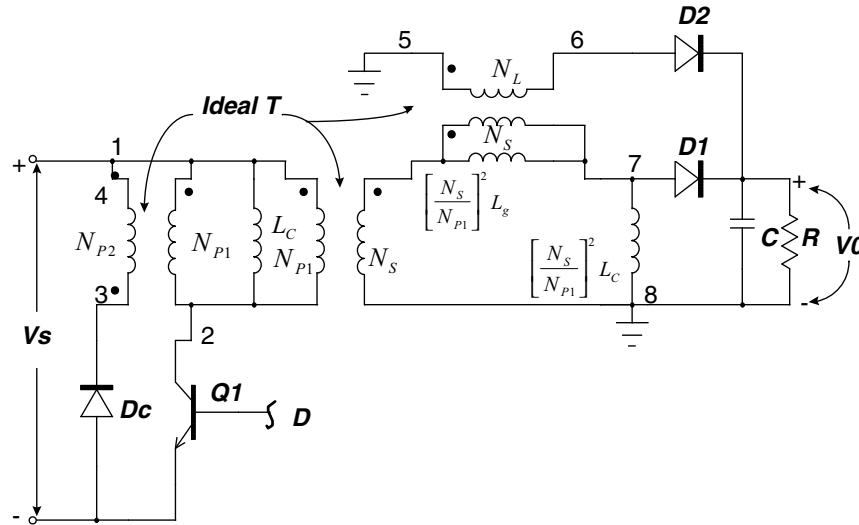


Figure 2.20 The completed forward converter shows how the reluctance derived transformer is integrated into the circuit.

### SPICE 2 Compatible Core Model

A saturable reactor is a magnetic circuit element consisting of a single coil wound around a magnetic core. The presence of a magnetic core drastically alters the behavior of the coil by increasing the magnetic flux and confining most of the flux to the core. The magnetic flux density,  $B$ , is a function of the applied MMF, which is proportional to ampere turns. The core consists of many tiny magnetic domains that are made up of magnetic dipoles. These domains set up a magnetic flux that adds to or subtracts from the flux that is set up by the magnetizing current. After overcoming initial friction, the domains rotate like small DC motors and become aligned with the applied field. As the MMF is increased, the domains rotate until they are all in alignment and the core saturates. Eddy currents are induced as the flux changes, thereby causing added loss.

A saturable core model that utilizes the PSpice subcircuit feature is available [76]. The saturable core subcircuit is capable of simulating nonlinear transformer behavior including saturation, hysteresis, and eddy current losses. To make the model even more useful, it has been parameterized. This is a technique that allows the characteristics of the core to be determined via the specification of a few key parameters. At the time of the simulation, the specified parameters are passed into the subcircuit. The equations in the subcircuit (inside the curly braces) are then evaluated and replaced with a value that makes the equation-based subcircuit compatible with PSpice.

```
.SUBCKT CORE 1 2 3
F1 1 2 VM1 1
G2 2 3 1 2 1
E1 4 2 3 2 1
VM1 4 5
RX 3 2 1E12
CB 3 2 {VSEC/500} IC={IVSEC/VSEC*500}
RB 5 2 {LMAG*500/VSEC}
RS 5 6 {LSAT*500/VSEC}
VP 7 2 250
D1 6 7 DCLAMP
VN 2 8 250
D2 8 6 DCLAMP
.MODEL DCLAMP D(CJO={3*VSEC/(6.28*FEDDY*500*LMAG)}
+ VJ=25)
.ENDS
```

**Figure 2.21** A netlist for a nonlinear magnetic core using SPICE 2 primitive elements.

The parameters that must be passed to the subcircuit include the following:

- Flux capacity in volt-seconds (VSEC)
- Initial flux capacity in volt-seconds (IVSEC)
- Magnetizing inductance in henries (LMAG)
- Saturation inductance in henries (LSAT)
- Eddy current critical frequency in hertz (FEDDY)

The saturable core may be added to a model of an ideal transformer to create a complete transformer model. To use the model, just place the core across the transformer's input terminals and specify the parameters. A special subcircuit test point has been provided to allow the monitoring of the core flux (node 3). Because there are two connections in the subcircuit, no connection is required at the top subcircuit level other than the dummy node number.

A sample PSpice call to the saturable core subcircuit looks similar to the following:

```
X1 2 0 3 CORE Params: VSEC = 50U IVSEC = - 25U LMAG = 10MHY
+ LSAT = 20UHY FEDDY = 20KHZ
```

The generic saturable core model is listed in Fig. 2.21.

### How the Core Model Works

Modeling the physical process performed by a saturable core is most easily accomplished by developing an analog of the magnetic flux. This is done by integrating the voltage across the core and then shaping

38 Chapter Two

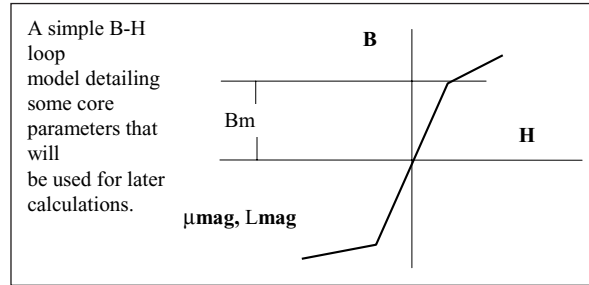


Figure 2.22 A simple B-H loop model detailing some core parameters that will be used for later calculations.

the flux analog with nonlinear elements to cause a current flow that is proportional to the desired function. This gives good results when there is no hysteresis, as illustrated in Fig. 2.22.

The input voltage is integrated using the voltage-controlled current source G and the capacitor CB (Fig. 2.23). An initial condition across the capacitor allows the core to have an initial flux. The output current from F is shaped as a function of flux using voltage sources VN and VP and diodes D1 and D2. The inductance in the high-permeability region is proportional to RB, while the inductance in the saturated region is proportional to RS. Voltages VP and VN represent the saturation flux. Core losses can be simulated by adding resistance across the input terminals; however, another equivalent method is to add capacitance across resistor RB in the simulation. Current in this capacitive element is differentiated in the model to produce the effect of resistance at the terminals. The capacitance can be made a nonlinear function of voltage,

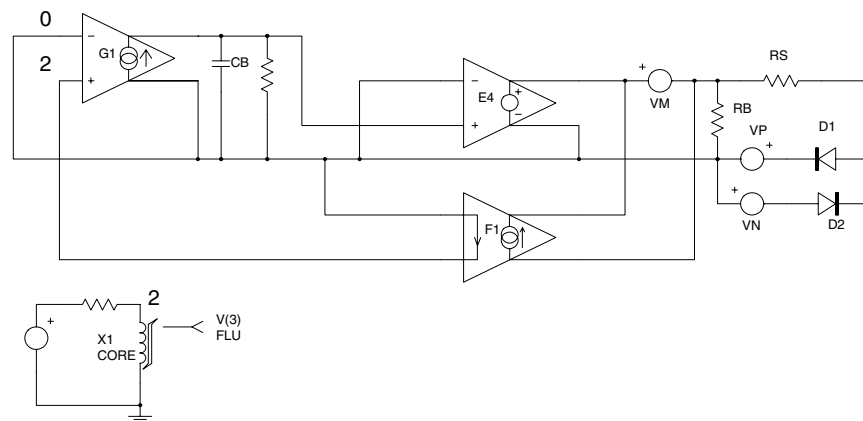


Figure 2.23 The saturable reactor model. The symbol below the schematic reveals the core's connectivity and subcircuit flux-density test point.

which results in a loss term that is a function of flux. A simple but effective way of adding the nonlinear capacitance is to specify a value for the diode parameter CJO. The other option is to use a nonlinear capacitor across nodes 2 and 6; however, the capacitor's polynomial coefficients are a function of saturation flux, thereby causing their recomputation if VP and VN are changed.

Core losses will increase linearly with frequency. A noticeable increase in MMF occurs when the core exits saturation, an effect that is more pronounced for square-wave excitation than for sinusoidal excitation, as shown in Fig. 2.25. These model properties agree closely with observed behavior [5]. The model is set up for orthonol and steel core materials that have a sharp transition from the saturated to the unsaturated region. The transition out of saturation is less pronounced for permalloy cores. To account for the different response, the capacitance value in the diode model (CJO in DCLAMP), which affects core losses, should be reduced. Also, reducing the levels of voltage sources VN and VP will soften the transition.

The DC B-H loop hysteresis, which is usually unnecessary for most applications, is not modeled because of the additional model complexity. This causes a prediction of lower loss at low frequencies. The hysteresis, however, does appear as a frequency-dependent function, as seen previously, and provides reasonable results for most applications, including magnetic amplifiers. The model in Fig. 2.23 simulates the core characteristics and takes into account the high-frequency losses associated with eddy currents and transient widening of the B-H loop, which is caused by magnetic domain angular momentum.

The saturable core model is capable of being used with both sine- (Fig. 2.24) and square- (Fig. 2.25) wave excitation. The circuit in Fig. 2.27 was used to generate the graphs.

### Calculating Core Parameters

The saturable core model is defined in electrical terms, thus allowing the engineer to design the circuitry without knowledge of the core's physical composition. After the design is completed, the final electrical parameters can be used to calculate the necessary core magnetic/size values. The core model may be altered so that it accepts magnetic and size parameters. The core could then be described in terms of  $N$ ,  $A_c$ ,  $Ml$ ,  $\mu$ , and  $B_m$ , and would be more useful for studying previously designed circuits. But the electrical model is better suited to the natural design process. The saturable core model's behavior is defined by the set of electrical parameters below. The core's magnetic/size values can be easily calculated from the following equations that use CGS units.

40 Chapter Two

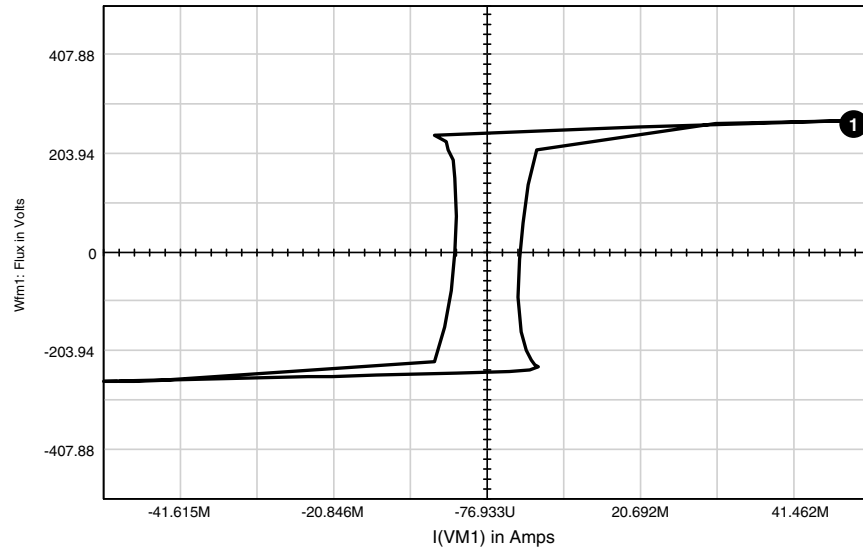


Figure 2.24 SPICE 2 syntax saturable core model under square-wave excitation.

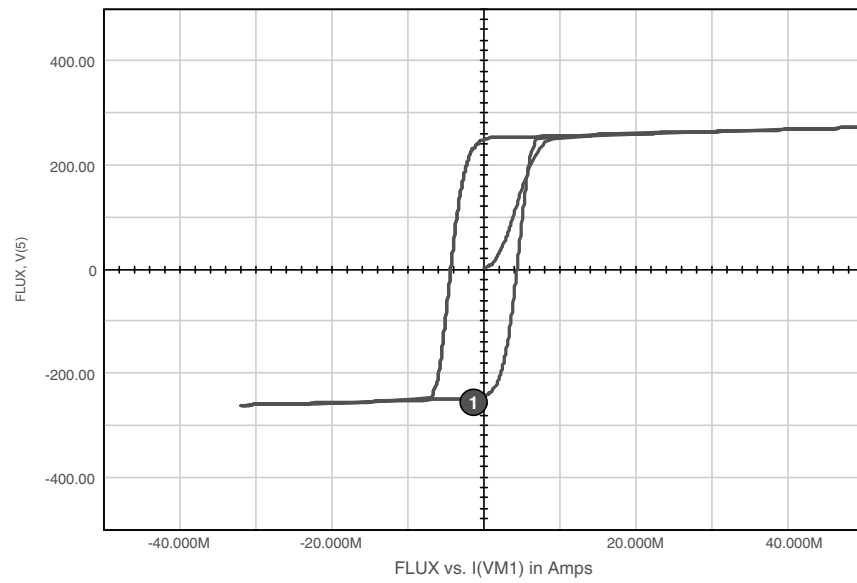


Figure 2.25 SPICE 2 syntax saturable core model under sine-wave excitation.



**Parameters passed to model**

VSEC Core capacity in volt-seconds  
 IVSEC Initial condition in volt-seconds  
 LMAG Magnetizing inductance in henries  
 LSAT Saturation inductance in henries  
 FEDDY Frequency when LMAG  
 Reactance = Loss resistance in hertz

**Equation variables**

$B_m$  Maximum flux density in gauss  
 $H$  Magnetic field strength in oersted  
 $A_c$  Area of the core in  $\text{cm}^2$   
 $N$  Number of turns  
 $l$  Magnetic path length in cm  
 $m$  Permeability

Faraday's law, which defines the relationship between flux and voltage, is given by the equation

$$E = N \frac{d\phi}{dt} \times 10^{-8} \quad (2.9)$$

where  $E$  is the desired voltage,  $N$  is the number of turns, and  $\phi$  is the flux of the core in Maxwell's equation. The total flux may also be written as

$$\phi_T = 2B_m A_c \quad (2.10)$$

Then, from Eqs. (2.9) and (2.10),

$$E = 4.44 B_m A_c F N \times 10^{-8} \quad (2.11)$$

and

$$E = 4.0 B_m A_c F N \times 10^{-8} \quad (2.12)$$

where  $B_m$  is the flux density of the material in gauss,  $A_c$  is the effective core cross-sectional area in  $\text{cm}^2$ , and  $F$  is the design frequency. Equation (2.11) is for sinusoidal conditions, while Eq. (2.12) is for a square-wave input. The parameter VSEC can then be determined by integrating the input voltage, resulting in

$$\int e dt = N\phi_T = N \times 2B_m A_c \times 10^{-8} = \text{VSEC} \quad (2.13)$$

42 Chapter Two

Also from  $E = L di/dt$ , we have

$$\int edt = Li \tag{2.14}$$

The initial flux in the core is described by the parameter IVSEC. To use the IVSEC option, you must put the UIC keyword in the “.TRAN” statement. The relationship between the magnetizing force and current is defined by Ampere’s law as

$$H = 0.4\pi N \frac{i}{Ml} \tag{2.15}$$

where  $H$  is the magnetizing force in oersteds,  $i$  is the current through  $N$  turns, and  $Ml$  is the magnetic path length in centimeters.

From Eqs. (2.13), (2.14), and (2.15) we have

$$L = N^2 B_m A_c \frac{(0.4 \pi \times 10^{-8})}{H \times Ml} \tag{2.16}$$

With  $\mu = B/H$ , we have

$$L_{(mag, sat)} = \mu_{(mag, sat)} N^2 \times 0.4 \pi \times 10^{-8} \times \frac{A_c}{Ml} \tag{2.17}$$

The values for LMAG and LSAT can be determined by using the proper value of  $\mu$  in Eq. (2.17). The values of permeability can be found by looking at the B-H curve and choosing two values for the magnetic flux: one in the linear region where the permeability will be maximum and one in the saturated region. Then, from a curve of permeability versus magnetic flux, the proper values of  $m$  may be chosen. The value of  $\mu$  in the saturated region will have to be an average value over the range of interest. The value of FEDDY, the eddy current critical frequency, can be determined from a graph of permeability versus frequency, as shown in Fig. 2.26. If we choose the approximate 3 dB point for  $\mu$ , we can determine the corresponding frequency.

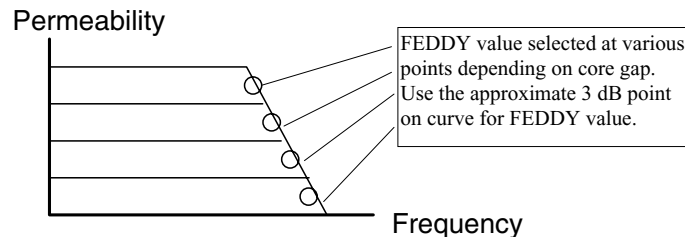


Figure 2.26 The permeability versus frequency graph is used to determine the value for FEDDY.

It should be noted that a similar core model can be constructed using generic physical parameters as opposed to generic electrical design parameters. For example,

```
.SUBCKT COREX 1 2 3 PARAMS: BI=0 N=1
RX 3 2 1E12
CB 3 2 {N*2*BR*ACORE*1E-8/500} IC={BI/BR*500}
F1 1 2 VM1 1
G2 2 3 1 2 1
E1 4 2 3 2 1
VM1 4 5
RB 5 2 {.625*N*UMAG/(LPATH * BR)*500}
RS 5 6 {.625*N*USAT/(LPATH * BR)*500}
VP 7 2 250
D1 6 7 DCLAMP
VN 2 8 250
D2 8 6 DCLAMP
* MULTIPLIER 3 AND VJ=25 GO TOGETHER
.MODEL DCLAMP D(CJO={3*LPATH * + BR/(6.28*FEDDY*500*.625*N*UMAG)}
VJ=25)
.ENDS
```

where the passed physical parameters are as follows:

ACORE	Magnetic cross-sectional area in $\text{cm}^2$
LPATH	Magnetic path length in cm
FEDDY	Frequency when $L_{\text{mag}}$ reactance = loss resistance
UMAX	Maximum permeability, $dB/dH$
USAT	Saturation permeability, $dB/dH$
BR	Flux density in gauss at $H = 0$ for saturated B-H loop
BI	Initial flux density, default = 0
N	Number of turns

### Using and Testing the Saturable Core

#### Saturable Core Test Circuit

```
.TRAN .1US 50US 0 .1US
.PROBE
.PRINT TRAN V(3) V(6) I(VM1) V(4)
R1 4 3 100
RL 2 0 50
X1 1 0 6 CORE Params: VSEC=25U IVSEC=-.25U LMAG=10MHY
+ LSAT=20UHY FEDDY=25KHZ
X3 3 0 2 0 XFMR Params: RATIO=.3
VM1 3 1
V2 4 0 PULSE -5 5 0US 0NS 0NS 25US
* Use the above statement for Square wave excitation
* V2 4 0 SIN 0 5 40K
* Use the above statement for Sin wave excitation
* Adjust Voltage levels to insure core saturation
.END
```

44 Chapter Two

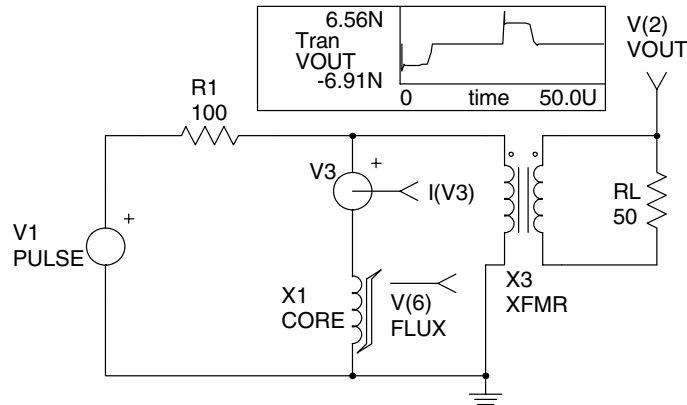


Figure 2.27 Saturable core test circuit schematic.  $I(V3) = I(VM1)$ .

The test circuit shown in Fig. 2.27 can be used to evaluate a saturable core model. Specify the core parameters in the curly braces and adjust the voltage levels in the “V2 4 0 PULSE” or “V2 4 0 SIN” statements to ensure that the core will saturate. You can use Eqs. (2.11) and (2.12) to get an idea of the voltage levels that are required in order to saturate the core. The .TRAN statement may also need adjustment, depending on the frequency that is specified by the V2 source. The core parameters must remain reasonable, or the simulation may fail. When the simulation is finished, you can plot V(5) versus I(VM1) (flux versus current through the core) to obtain a B-H plot.

An improved version of this model, adding low-frequency hysteresis [100, 101], is shown below.

```
.SUBCKT CORE 1 2 3
DH1 1 9 DHYST
DH2 2 9 DHYST
IH1 9 1 {IHYST}
IH2 9 2 {IHYST}
F1 1 2 VM 1
G1 2 3 1 2 1
E1 4 2 3 2 1
VM 4 5
C1 3 2 {SVSEC/250} IC={IVSEC/SVSEC * 250}
RB 5 2 {LMAG * 250/SVSEC}
RS 5 6 {LSAT * 250/SVSEC}
VP 7 2 250
D1 6 7 DCLAMP
VN 2 8 250
D2 8 6 DCLAMP
E2 10 0 3 2 {SVSEC/250}
.MODEL DHYST D
.MODEL DCLAMP D(CJO={3 * SVSEC/(250 * REDDY)} + VJ=25)
.ENDS
```

where

SVSEC	Volt-sec at saturation = $B_{\text{SAT}} \cdot A_E \cdot N$
IVSEC	Volt-sec initial condition = $B \cdot A_E \cdot N$
LMAG	Unsaturated inductance = $\mu_0 \mu_R \cdot N^2 \cdot A_E / L_M$
LSAT	Saturated inductance = $\mu_0 \cdot N^2 \cdot A_E / L_M$
IHYST	Magnetizing I @ 0 flux = $H \cdot L_M / N$
REDDY	Eddy current loss resistance

SVSEC and IVSEC are based on peak flux values. LMAG: For an ungapped core,  $L = L_M$  (total path around core); for a gapped core,  $\mu_R = 1$ ,  $L = \text{gap length}$ ,  $A_E = \text{core area (m}^2\text{)}$ . LSAT: Use core dimensions but with  $\mu_R = 1$ . REDDY: Equals LMAG reactance when permeability versus frequency is 3 dB down.

Magnetizing current associated with low-frequency hysteresis is provided by current sinks IH1/IH2. With no voltage across terminals 1 and 2, these currents circulate through their respective diodes, and the net terminal current is zero. When voltage is applied, the appropriate diode starts to block and its current sink becomes active.

### SPICE 3 Compatible Core Model

A magnetic core model has three major elements: permeability, hysteresis, and core loss. Unfortunately, both the permeability and the core loss are nonlinear functions. The models in this chapter properly represent the nonlinear permeability and the hysteresis. The core loss has not been modeled in this SPICE 3 version.

The model is based upon the premise that a magnetic element is represented by an inductance. The inductance is related to the permeability and geometrical properties of the core. The current through the inductor can then be simply stated as

$$I = \frac{1}{L} \int V dt$$

This function can be modeled as a simple integrator. To properly represent the B-H loop characteristics, the nonlinearities of the inductance need to be defined.

Fortunately, graphical data are available that provide the percentage of initial permeability versus DC bias for several core types. Using curve-fitting techniques, the nonlinear permeability can be approximated in closed-loop form. The nonlinear permeability can then be used to modify the slope of the integrator. The resulting equation, which we

46 Chapter Two

will model, is

$$I = \frac{1}{L \times \%U} \int V dt$$

The results have shown that the B-H characteristics properly represent the hysteresis and remanance effects of the core. Core loss must be represented at a single operating condition or may be entered outside of the model. This can be accomplished via the use of parameter passing. In this case, the 3-dB point on the permeability versus frequency graph was used. The configuration of the model is shown in Fig. 2.28.

In PSpice, the SPICE 3 B-elements are replaced by voltage-controlled voltage or current source equivalents (E or G elements). B1 calculates the magnetizing force in the inductor using the relationship

$$H = \left| \frac{0.4 \pi NI}{l_m} \right|$$

where  $N$  is the number of turns,  $I$  is the current through the element (measured by V1), and  $l_m$  is the magnetic path length of the core. Because  $H$  is a real value, its absolute value is used. B2 calculates the percent permeability using the equation defined above. B3 calculates the voltage across the element, divided by the percent permeability.

G1 integrates the value of BS3 and presents it to G2, which forces a current flow through the element. With the values of G1 and G2 both established as 1, the current through the element is

$$I = \frac{1}{C \times \%U} \int V dt$$

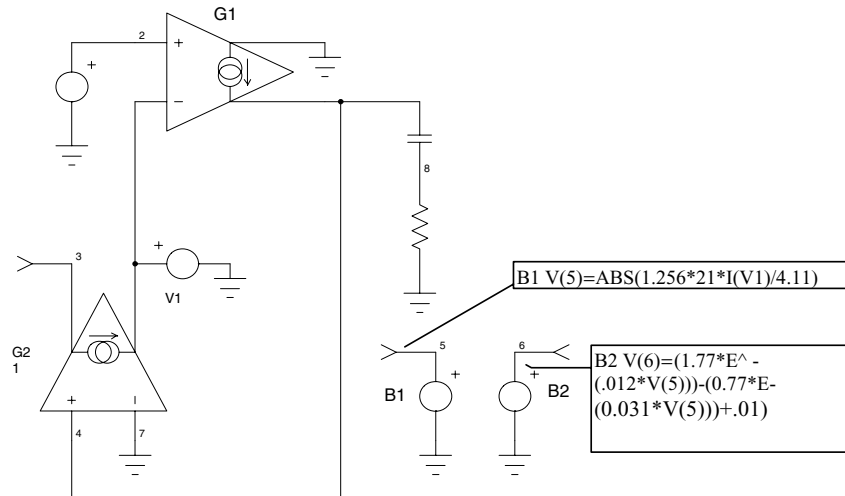


Figure 2.28 Schematic of the SPICE 3 core model. V(6) = % Permeability, V(5) = H.

Because this is in the desired form, we can solve for all of the variables.

**Example 1—MPP core**

Using the permeability versus DC bias data provided by Magnetics<sup>®</sup>, multiple iterations and curve-fitting techniques, a closed form solution for the 60u material was found to be approximated by

$$\%U_i = 1.77e^{-.021H} - 0.77e^{-.031H}$$

where  $U_i$  is the initial inductance of the core and  $H$  is the magnetizing force in oersteds.

$$C = L = \left( \frac{N}{1000} \right)^2 A_L$$

where  $A_L$  is the inductance reference of the core.

$$B_1 = \left| \frac{0.4\mu NI(VI)}{l_m} \right|$$

$$B_2 = 1.77e^{-.012V(B_1)} - 0.77e^{-.031V(B_1)} + 0.02$$

$$B_3 = \frac{V(3, 4)}{V(B_2)}$$

$$R_2 = \frac{1}{2\pi f_{\text{eddy}}C}$$

The following circuit uses the above derivation to model a Magnetics<sup>®</sup> 55121 MPP core with 21 turns. The constants given in the data book for the 55121 core provide the following values:  $A_L=35$  mH,  $l_m=4.11$  cm, core weight=0.015 lb,  $f_{\text{eddy}}= 7$  MHz, and  $U_i=60$ . We can calculate the components of the model as

$$C = \left( \frac{21}{1000} \right)^2 \times 35 \text{ mH} = 15.4 \mu\text{F}$$

$$B_1 = \left| \frac{0.4\pi (21) I(V_1)}{4.11} \right|$$

$$R_1 = \frac{1}{2\pi (7 \text{ MHz}) (15.4 \mu\text{F})} = 0.0015$$

The SPICE netlist is provided later (Fig. 2.29). Note that  $R_1$  represents the winding's DC resistance. The test circuit sweeps the current

## 48 Chapter Two

```

MPP: MODELING A MAGNETICS®55121 MPP CORE
* PSpice version
.DC II .1 100 .10
.AC DEC 20 100HZ 10MEGHZ
.PROBE
.PRINT AC V(4) VP(4)
* Node 4 Impedance
.PRINT DC V(6) V(5)
* Node 6 = H, Node 5 = % Permeability
G2 3 1 9 0 1
V1 1 0
G1 0 9 2 1 1
C1 9 8 15.4U
R2 8 0 1.5M
E1 5 0 Value = { ABS(1.256*21*I(V1)/4.11) }
E2 6 0 Value = { (1.77*Exp(-.012*V(5)))-(.77*Exp(-.031*V(5)))+.01 }
E3 2 0 Value = { V(3,1)/V(6) }
I1 0 4 AC 1
R1 4 3 .04
RT4 4 0 1G
RT3 3 0 1G
RT9 9 0 1G
.END
  
```

**Figure 2.29** Netlist for a 55121 MPP core.

through the “core” while the percent permeability and magnetizing force are monitored and displayed in Fig. 2.30. Actual data points are plotted as dots, while the calculated results are plotted using line style. An AC impedance plot is also performed (Fig. 2.31). Calculating the inductance from the impedance curve yields

$$L = \frac{1}{2\pi (10.19 \text{ kHz})} = 15.6 \mu\text{H}, \text{ which agrees with the expected } 15.4 \mu\text{H}.$$

The percent permeability versus magnetizing force curve was integrated and multiplied by the initial permeability [59]. The resulting graph is the DC B-H curve shown in Fig. 2.32. The curve shows a maximum flux density of approximately 7500 G, which agrees with the specified value of 7000 G.

### Ferrite Cores

The same principles apply to ferrite cores as well as MPP cores. In this example, a model is generated for ferrite “F” material. Again, trial-and-error and curve-fitting techniques may be used in order to obtain a closed-form expression of percent permeability versus magnetizing force. Graphical data are provided in the Magnetism Ferrite Data Book.



SPICE Modeling of Magnetic Components 49

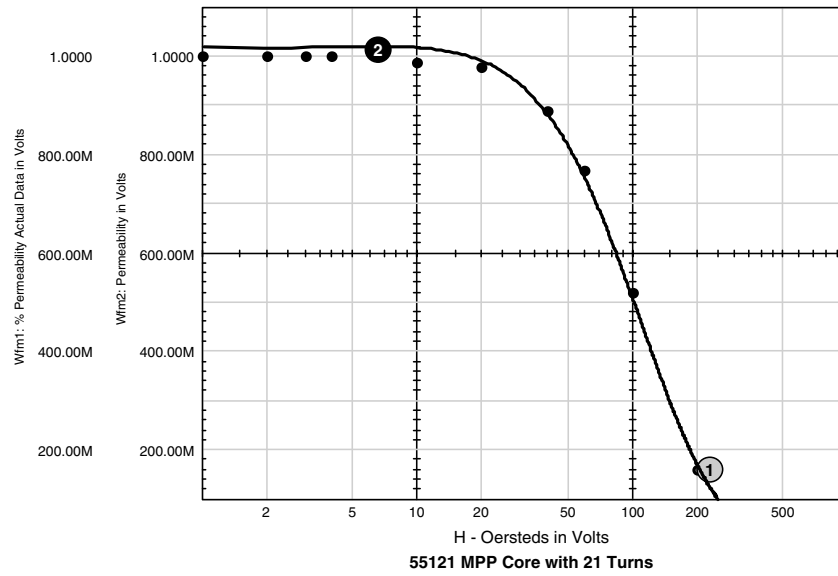


Figure 2.30 Permeability versus magnetizing force.

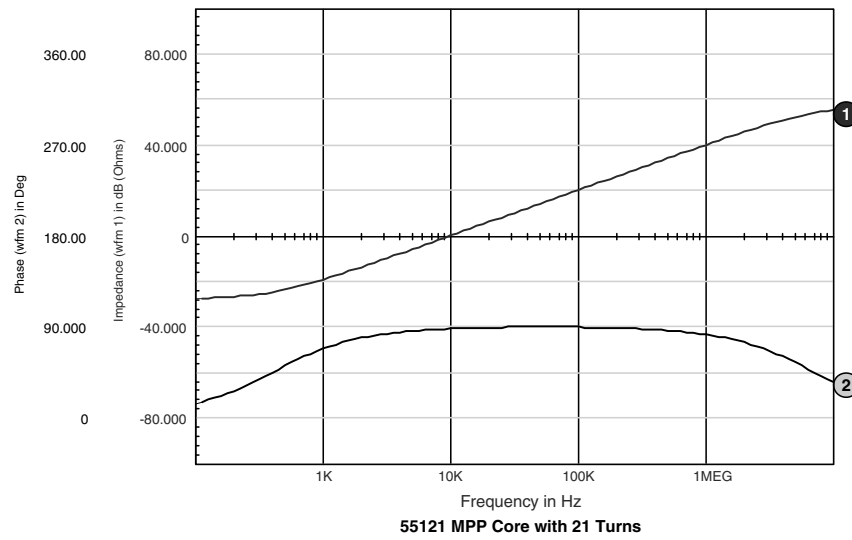


Figure 2.31 Impedance for the 55121 core.

50 Chapter Two

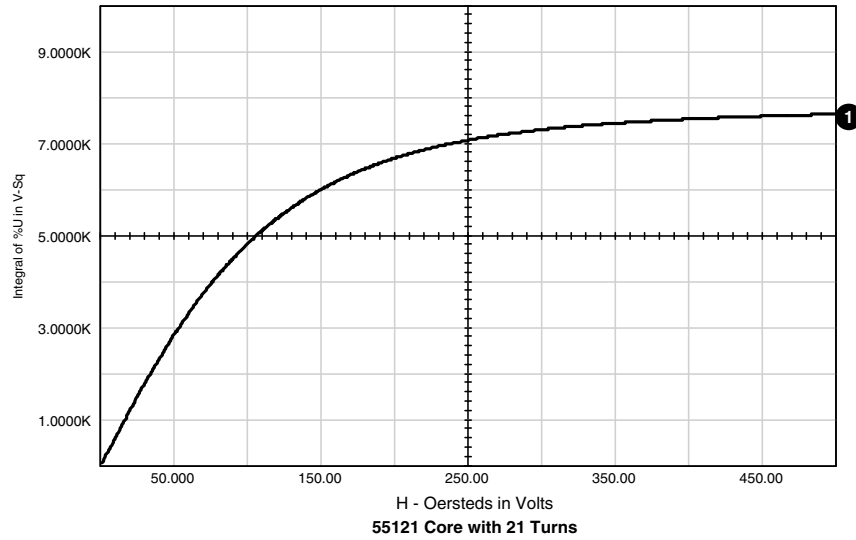


Figure 2.32 DC B-H curve.

Although the MPP model is represented using exponential functions, the ferrite model is much more accurately represented via a power function. The resulting expression for ferrite “F” material is

$$%U = \frac{1.149 \times 1.09H^{-1.1376}}{1.05 + 1.094H^{-1.1376}}$$

The result of the  $%U$  calculation was multiplied by the initial permeability (3000) in order to obtain the same terms as those contained in the Ferrite Data Book.

The graph below shows the actual permeability versus magnetizing force. Actual data points are plotted as dots, while the calculated results are plotted using line style (Fig. 2.33).

**Example 2—Ferrite core**

As an example, a model was created for an F2213 pot core with 1 turn. The data sheet parameters for the F2213 pot core defines the values as follows:  $A_L=4900$  mH,  $l_m=3.12$  cm,  $U_i= 3000$ , and  $f_{eddy}=1$  MHz. The schematic in Fig. 2.34 shows the circuit model for the core.

The basic structure of the model is very similar to that of the MPP core model. The major differences lie in the definition of the nonlinear  $B_2$  and the fact that the core loss is shown as a parallel resistor rather than a series resistor. Also, note that a resistor is not added to

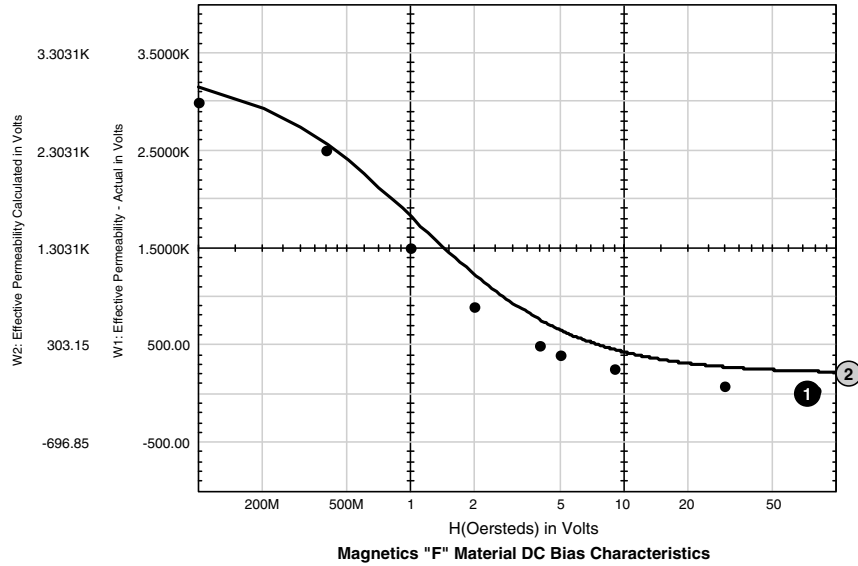


Figure 2.33 Permeability versus magnetizing force.

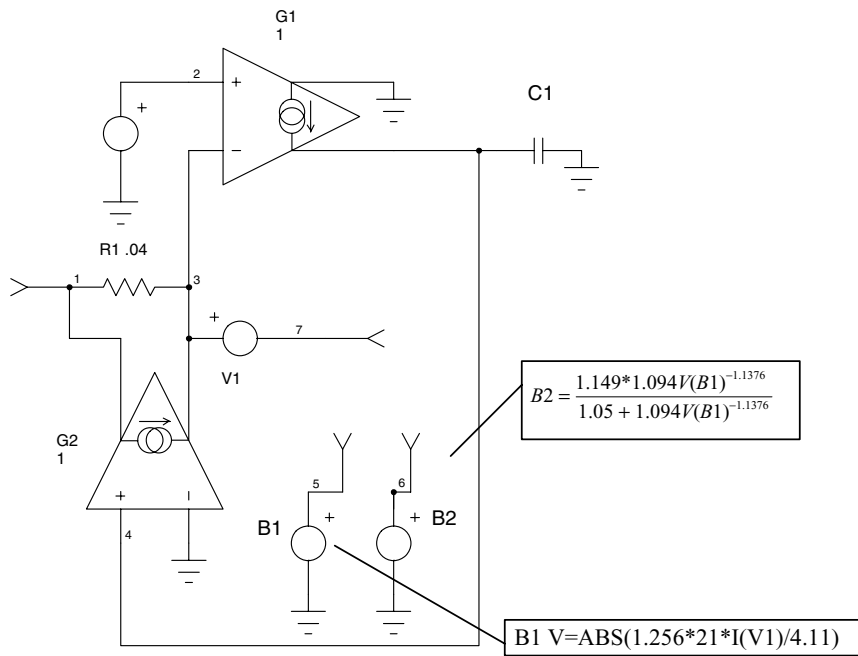


Figure 2.34 Schematic for the F2213 pot core. V(6) = %Permeability, V(5) = H.

52 Chapter Two

represent DC resistance (DCR), because it would be a property of the winding.

$$B_1 = \left| \frac{0.4 \pi (1) I (V_1)}{3.12} \right| = 0.4026I (V_1)$$

$$C_1 = \left( \frac{1}{1000} \right)^2 \times 4900 \text{ mH} = 4.9 \mu\text{F}$$

$$B_3 = \frac{V(3, 4)}{V(B_2)}$$

$$B_2 = \frac{1.149 \times 1.094V(B_1)^{-1.1376}}{1.05 + 1.094V(B_1)^{-1.1376}}$$

$$R_1 = 2\pi f_{\text{eddy}}C_1 = 30.77 \Omega$$

A test circuit is required in order to generate the B-H loop curve. A pulse source is used to excite the core through a limiting resistor. The flux level and magnetizing force,  $H$ , must be measured. To measure the flux level, we can use the following form of Maxwell's equation:

$$\text{Flux} = \frac{Vt \times 10^8}{A_c N}$$

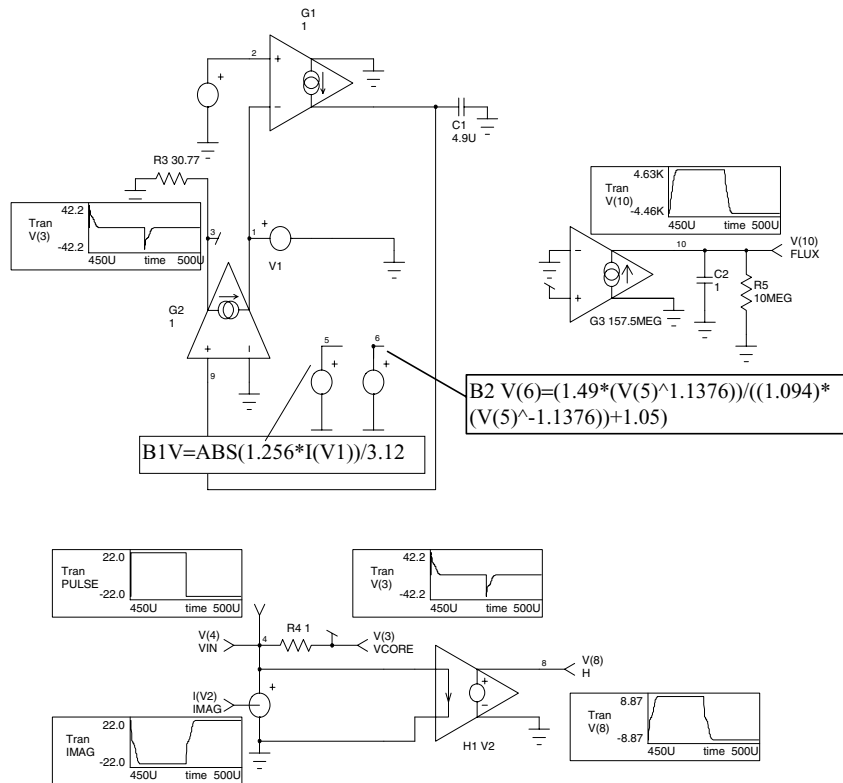
where  $A_c$  is the core area in  $\text{cm}^2$  and  $N$  is the number of turns.

If we use a voltage-controlled current source with a gain of 1, we can charge a 1-F capacitor and scale the capacitor voltage by a factor of

$$\frac{10^8}{A_c N}$$

The core area is given in the data sheet as  $0.635 \text{ cm}^2$ , which calculates to a scaling factor of  $157.5 \times 10^6$ . We could use the magnetizing force that was calculated by  $B_1$ , but we took its absolute value. We will use a current-controlled voltage source to measure the excitation current because we can define the scaling factor as  $\frac{0.4 \pi}{3.12} I = 0.403I$ . The completed model, including the test circuit, is shown in Fig. 2.35.

The circuit was simulated and an X-Y plot was created. The results are shown in Fig. 2.36. The curve agrees with the Magnetics B-H loop data. The pulse voltage waveform and the core voltage waveform are also shown.



MAGF: TEST CIRCUIT TO GENERATE THE B-H LOOP CURVE

```

*Pspice version
.TRAN .1U 500U 450U .1U UIC
.PROBE
*I(V2)=IMAG
*V(10)=FLUX
*V(8)=H
*V(3)=VCORE
*V(4)=PULSE
.PRINT TRAN V(4) I(V2) V(10) V(8)
V1 1 0
G1 1 0 9 2 1 1
C1 1 9 0 4.9U IC=0
E1 5 0 Value={ ABS(1.256*I(V1))/3.12 }
E2 6 0 Value={ (1.149*(V(5)^-1.1376))/((1.094*(V(5)^-1.1376))+1.05) }
E3 2 0 Value={ V(3,1)/(V(6)+.001) }
Vin 4 0 PULSE -20 20 10N 10N 10N 25U 50U
R3 3 0 30.77
R4 4 3 1
G3 0 10 3 0 157.5MEG
C2 10 0 1 IC=0
R5 10 0 10MEG
H1 8 0 V2 -.403
G2 3 1 9 0 1
RT9 9 0 1G
.END
    
```

Figure 2.35 Schematic test circuit and net list for the F2213 pot core.

54 Chapter Two

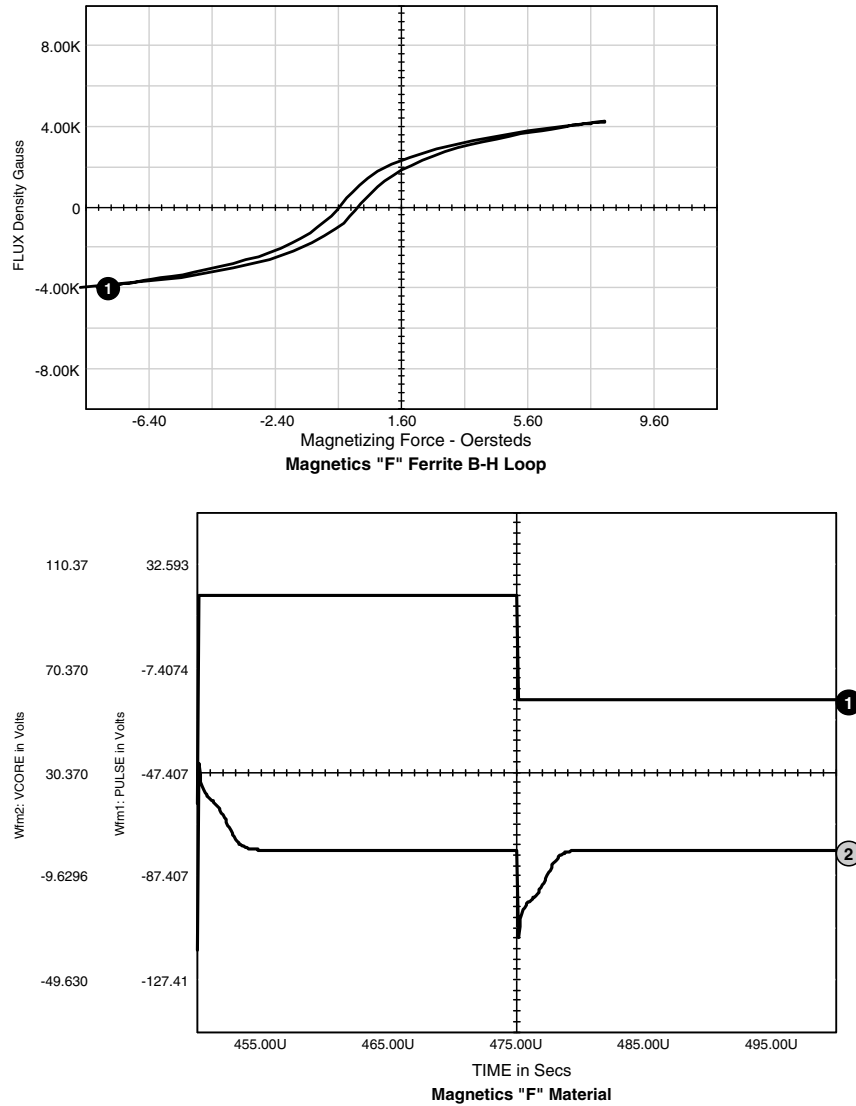
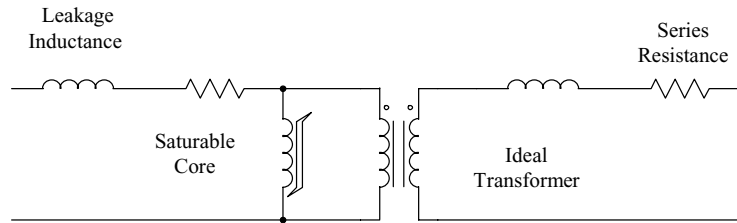


Figure 2.36 B-H loop for the F2213 pot core (top) and pulse waveform response (bottom).

### Constructing a Transformer

As a final exercise in this chapter, we will combine the core model which we just completed, along with the turns subcircuit, and model a two-winding transformer.

To make a transformer model that more closely represents the physical processes, it is necessary to construct an ideal transformer and



**Figure 2.37** A complete transformer model. The saturable core may be combined with the ideal transformer, XFMR, and some leakage inductance and series resistance to create a complete model of a transformer.

model the magnetizing and leakage inductances separately. The ideal transformer was discussed previously in this chapter. It has a unity coupling coefficient and infinite magnetizing inductance.

The magnetizing inductance is added by placing the saturable reactor model (suitably scaled) across any one of the windings. Coupling coefficients are inserted in the model by adding the series leakage inductance for each winding as shown in Fig. 2.37.

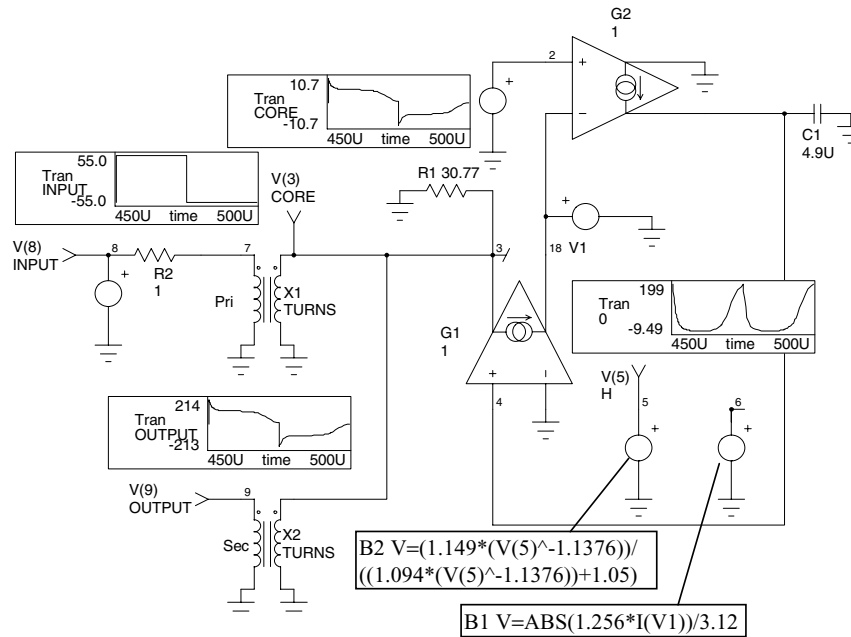
The leakage inductances are measured by finding the short-circuit input inductance at each winding and then solving for the individual inductance. These leakage inductances are independent of the core characteristics, as shown in reference [102]. The final model, incorporating the saturable core model and an ideal transformer subcircuit, along with the leakage inductance and winding resistance, is shown in Fig. 2.37.

PSpice models cannot represent all possible behavior because of the limits of computer memory and run time. This model, as most simulations, does not represent all cases.

Modeling the core as a single element referred to one of the windings works in most cases; however, some applications may experience saturation in a small region of the core, causing some windings to be decoupled faster than others, invalidating the model. Another limitation of this model is for topologies with magnetic shunts or multiple cores. Applications like this can frequently be solved by replacing the single magnetic structure with an equivalent structure using several transformers, each using the model presented here.

Another example is shown in Fig. 2.38. The SPICE 3 core model remains unchanged. We have simply added two transformer (turns) subcircuits. The primary winding has 10 turns, and the secondary has 20 turns. The secondary of the turns subcircuit is always 1 turn, which is the reason that we developed the core with 1 turn. The circuit was stimulated with a 10-V peak 20-kHz square-wave voltage applied through a 1- $\Omega$  series resistor, and also with a 50-V peak 25-kHz square-wave voltage.

56 Chapter Two



EX5: MODEL FOR A TWO-WINDING TRANSFORMER

```

*Pspice version
.AC DEC 20 100HZ 10MEGHZ
.TRAN .1U 500U 450U UIC
*V(9)=OUTPUT
*TM(3)=CORE
*V(8)=INPUT
*V(5)=H
.PRINT AC V(9) VP(9) V(3) VP(3)
.PRINT AC V(8) VP(8)
.PRINT TRAN V(9) V(3) V(8) V(5)
V1 1 0
G2 0 4 2 1 1
C1 4 0 4.9U IC=0
E1 5 0 Value = { ABS(1.256*I(V1))/3.12 }
E2 6 0 Value = { (1.149*(V(5)^-1.1376))/((1.094*(V(5)^-1.1376))+1.05) }
E3 2 0 Value = { V(3,1)/(V(6)+.001) }
R1 3 0 30.7700
X1 7 0 3 0 TURNS Params: NUM=10
X2 9 0 3 0 TURNS Params: NUM=20
*Turns is similar to XFMR except Ratio = 1/Num
V2 8 0 AC 1 PULSE -50 50 1N 1N 1N 25U 50U
R2 8 7 1
G1 3 1 4 0 1
RT4 4 0 1G
.END

```

Figure 2.38 Schematic and netlist for the two-winding transformer test circuit.



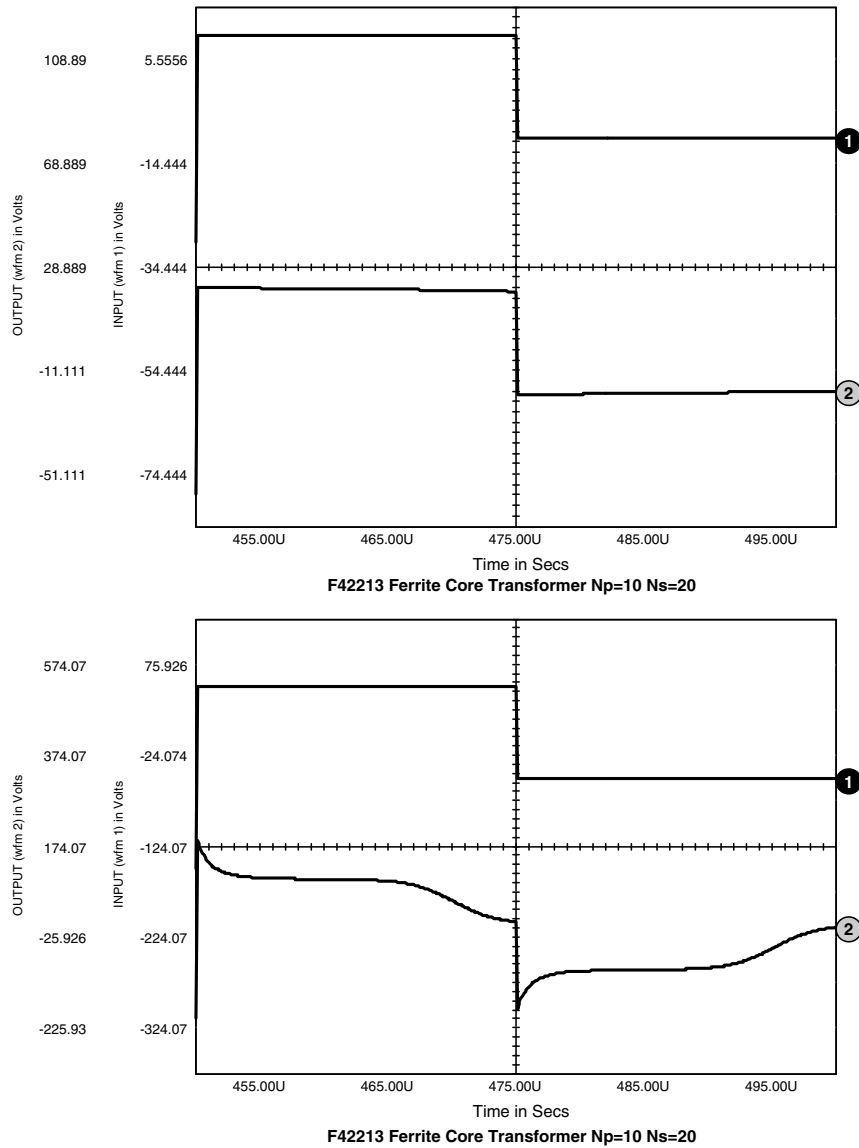


**Figure 2.39** Input and output voltages for the complete transformer circuit (top), transient core saturation characteristics (bottom).

The input and output voltage of the transformer are shown in Fig. 2.39. Note that the output voltage agrees with the turns ratio, for it is twice the level of the input voltage. The second plot illustrates the core saturation characteristics, which are represented by the B-H loop.

### High-Frequency Winding Effects

Winding resistance can be modeled by adding a series resistance to each winding as shown in Fig. 2.40. At low frequencies  $R_w$  is simply the DC resistance of the winding. At the higher frequencies more common in power conversion, however, the winding resistance is more complex because of the presence of skin and proximity effects within the windings.

There are several reasons for wanting to correctly model the winding resistance:

- Reproduce the winding loss.
- Reproduce the effect of winding resistance on voltage drop within and cross-regulation between windings.
- Reproduce the damping effect that the winding resistance will have on parasitic ringing.

To achieve these goals, it is necessary to determine the effective resistance, including the high-frequency effects.

Procedures for estimating winding resistance are well known and can be used to establish model parameters. A typical graph of winding resistance versus frequency for windings with different numbers of layers is given in Fig. 2.41. The graph is normalized for a 1- $\Omega$  DC resistance and a frequency where the layer thickness is 1 skin depth ( $\delta$ ):

$$\delta_{\text{CU}} = \frac{0.661}{\sqrt{\pi \mu \sigma f_s}} \text{ m}$$

The current waveform in the winding is assumed to be a sine wave. The key feature of the graph is the rapid increase in resistance above a corner frequency that is determined by the number of layers. The winding resistance is frequency dependent and the change in resistance can be quite large.

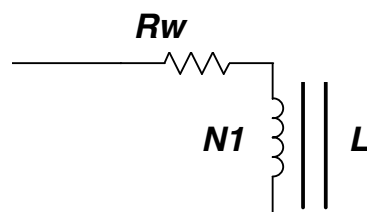


Figure 2.40 Winding resistance model.

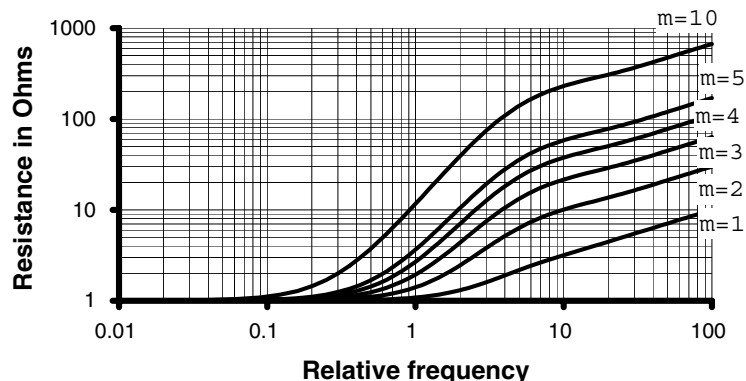


Figure 2.41 HF winding resistance, normalized to  $1 \Omega (R_{dc})$  at frequency where the layer is 1 skin depth thick.

The winding resistance is also dependent upon the shape of the current waveform. Figure 2.42 is an example of a three-layer winding with a symmetrical bipolar PWM current waveform. Note that all square wave duty cycles produce a result greater than a sine wave, which is also plotted for comparison. This is due to the harmonic content of the waveform. Also note that as the duty cycle ( $D$ ) is varied from a square wave ( $D = 0.5$ ) to a smaller duty cycle, the winding resistance first decreases and then increases as it becomes quite large at low duty cycle values. This seemingly bizarre behavior is due to the changing harmonic spectrum as the duty cycle is modulated.

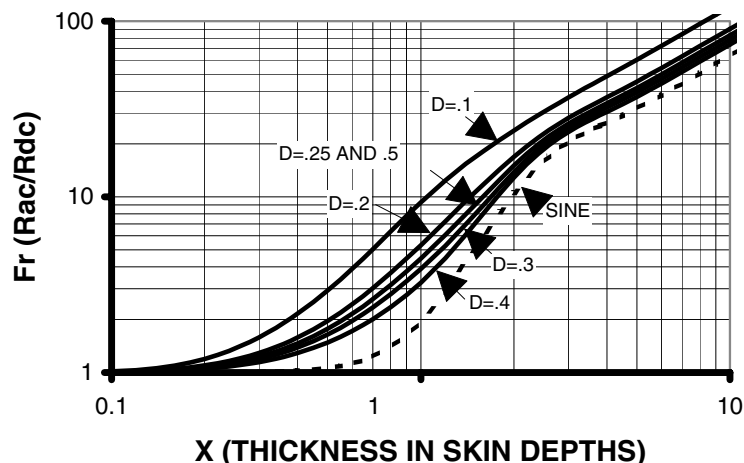


Figure 2.42  $F_r$  for a bipolar PWM current ( $m=3$ ).

60 Chapter Two

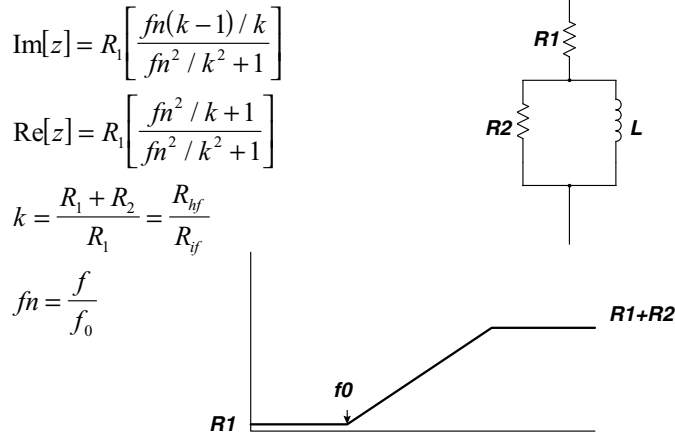


Figure 2.43 A resistance that varies with frequency can be simulated with a network of linear components.

In a typical high-frequency power converter, the winding resistances will vary as a function of frequency, modulation, load distribution between the windings, and temperature. In general, it is not practical or necessary to model all of these effects, but there are some useful approximations.

If winding loss is the most important concern, then the winding resistance can be represented by a simple series resistor in each winding, the values of which are chosen to represent the effective AC resistance at the highest loss condition of load, duty cycle, and temperature. This choice will overstate the loss at other conditions, but it is usually preferable to understatement under the worst-case conditions.

It is possible to approximate a frequency variable resistor with a network of linear components, as shown in Fig. 2.43. At low frequencies, the inductor is essentially a short circuit and  $R = R_1$ . At high frequencies, the inductor is an open circuit and  $R = R_1 + R_2$ . The change in resistance follows the single-pole asymptotic approximation, which is shown in the graph in Fig. 2.43. The equations for the real and imaginary components of the network driving point impedance ( $z$ ) are also given.

A graph of the real part of  $z$  is given in Fig. 2.44 for different resistance ratios. For a suitable choice of  $f_0$  and  $k$ , the change of resistance can be modeled over a substantial frequency range.

There is, however, an important limitation associated with this network. The ratio of the real and imaginary parts of  $z$  is plotted as a graph in Fig. 2.45.

Because of the presence of the inductor in the network, there will be some inductive reactance. As shown by the graph, this peaks between

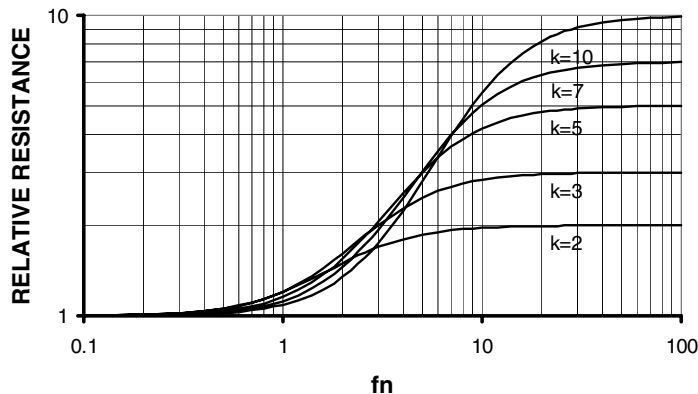


Figure 2.44 Graph of  $Re[z]$  for different resistance ratios.

the upper and lower resistive break points. For small resistance ratios, the inductive reactance is relatively small, but as the ratio gets larger, the inductance becomes significant and this simple network is no longer just a variable frequency resistor but is also a variable frequency inductor. This may not be a problem if a series inductor is being used to simulate the leakage inductance of the winding. If the leakage inductance is large enough, it may mask the network inductance sufficiently so that its effect can be ignored.

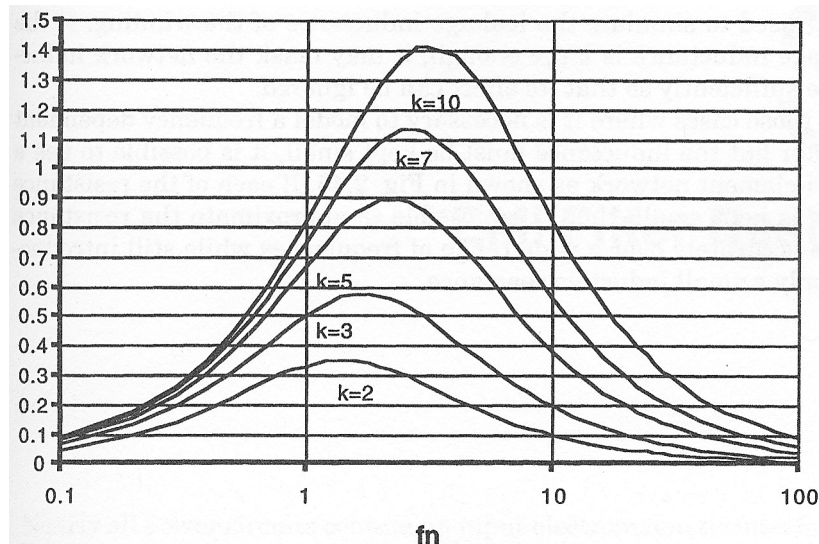


Figure 2.45 Graph of  $Im[z]/Re[z]$  for different resistance ratios.

62 Chapter Two

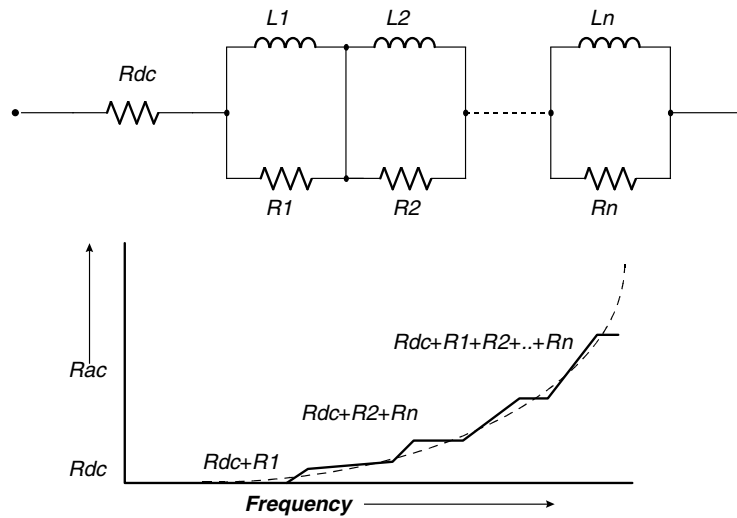


Figure 2.46 High-frequency resistance model using a multielement network.

In cases where it is necessary to model a frequency-dependent resistor but the inductance must be kept small, it is possible to use a multielement network as shown in Fig. 2.46. If each of the resistance steps is kept small, then it is possible to approximate the resistance quite accurately over a wide range of frequencies while still introducing only a small inductive reactance.